nature communications

Article

https://doi.org/10.1038/s41467-025-64773-5

PROTAC repurposing uncovers a noncanonical binding surface that mediates chemical degradation of nuclear receptors

Received: 28 February 2025

Accepted: 26 September 2025

Published online: 06 November 2025

Check for updates

Andrew D. Huber[1], Wenwei Lin[1], Young-Hwan Jung[1], Shyaron Poudel[1], Guangwei Yang[1], Jing Wu[1], Annalise G. Carrigan[1], Vishwajeeth Pagala[2], Wei Wang[2], Yingxue Fu[2], Zuo-Fei Yuan[2], Stephanie D. Byrum[2], Ka Yang[3], Rebecca R. Florke Gee[1,4], Elizabeth D. Arnold[5,6], Allister J. Loughran[5,6], Jingheng Wang[1], Shondra M. Pruett-Miller[5,6], Junmin Peng[3,7] & Taosheng Chen[1]

Proteolysis-targeting chimeras (PROTACs) containing a target protein ligand linked to an E3 ubiquitin ligase ligand induce target protein degradation through E3 recruitment. Most PROTACs bind a surface cleft of the protein of interest rather than a buried pocket. Using the nuclear receptor PXR, we previously described the inherent difficulties of PROTAC targeting via a deep solvent-inaccessible ligand binding pocket. Here, we discover that the CRBN-dependent MDM2 PROTAC MD-224 is a potent PXR degrader that achieves its activity from binding adjacent to the ligand-binding pocket. Furthermore, because the proximal region is a structural feature common among nuclear receptors, MD-224 also targets additional receptors for proteasomal degradation. Using structure- and activity-guided medicinal chemistry, we ablated MDM2 degradation and generated MD-224 analogs with activities skewed toward different receptors. Thus, we describe (1) PROTAC repurposing as a potential route of degrader discovery and (2) nuclear receptor-targeted degradation through a noncanonical binding site.

Transcription factors are essential components of cellular processes, including division, differentiation, disease, and senescence. More than 1,600 likely transcription factors are encoded by the human genome, and >300 are currently associated with at least one disease phenotype[1]. Classically described as undruggable proteins due to their multidomain or disordered structures that often lack clear ligand binding pockets[2,3], transcription factors have gained much therapeutic attention in the past decade due to the advent of chemically tunable protein degradation. Specifically, the immunomodulatory drug thalidomide and its analogs were shown to recruit transcription factors IKZF1 and IKZF3 to the CUL4-RBX1-DDB1-CRBN ($CRL4^{CRBN}$) E3 ubiquitin ligase, resulting in their ubiquitination and degradation[4–6]. These compounds act by a "molecular glue" mechanism, inducing a protein-protein interaction between CRBN and IKZF1/3[7]. Subsequent linkage of thalidomide to various target protein ligands resulted in proteolysis targeting chimeras (PROTACs) that specifically induce degradation of a range of proteins, such as the epigenetic readers BRD2, BRD3, and BRD4[3]. While the PROTAC concept has long been studied[8], it has only recently gained traction as a viable therapeutic option due, in part, to the discoveries of specific E3 ubiquitin ligase ligands such as

[1]Department of Chemical Biology and Therapeutics, St. Jude Children's Research Hospital, Memphis, TN, USA. [2]Center for Proteomics and Metabolomics, St. Jude Children's Research Hospital, Memphis, TN, USA. [3]Department of Structural Biology, St. Jude Children's Research Hospital, Memphis, TN, USA. [4]Graduate School of Biomedical Sciences, St. Jude Children's Research Hospital, Memphis, TN, USA. [5]Department of Cell and Molecular Biology, St. Jude Children's Research Hospital, Memphis, TN, USA. [6]Center for Advanced Genome Engineering, St. Jude Children's Research Hospital, Memphis, TN, USA. [7]Department of Developmental Neurobiology, St. Jude Children's Research Hospital, Memphis, TN, USA. e-mail: taosheng.chen@stjude.org

thalidomide. PROTACs are distinct from molecular glues in that they are bivalent molecules with an E3 ubiquitin ligase ligand linked to a ligand for the protein of interest; molecular glue-type degraders, on the other hand, are monovalent and facilitate specific protein-protein interactions[7].

Nuclear receptors (NRs) are unique among transcription factors due to the presence of dedicated ligand binding domains (LBDs) that allow modulation of transcriptional transactivation by small molecules[9]. Due to these defined LBDs, NRs form a privileged family that is targeted by 16% of approved small molecule drugs[10], but considerable overlap of NR ligand binding profiles leads to undesirable off-target effects and hinders progress of new NR-targeting drugs. Furthermore, unexpected events such as tissue-specific activation of estrogen-dependent genes by antiestrogens[11] have long reinforced the need for NR modulators that act by distinct mechanisms. One of these mechanisms is induced degradation of the target receptor, such as selective estrogen receptor (ER) downregulators described as early as 1992[12], but the mechanisms by which the molecules act remain elusive[13]. The use of PROTACs has made NR degradation more controllable, and PROTACs have been synthesized for multiple receptors, including ERs[14], estrogen-related receptor alpha (ERRα)[15], androgen receptor (AR)[16], and liver X receptor beta (LXRβ)[17]. However, we recently reported the difficulty of designing PROTACs to target receptors with deep, poorly accessible pockets, such as pregnane X receptor (PXR)[18,19].

PXR functions as a xenobiotic receptor, recognizing structurally diverse drugs and upregulating drug metabolism enzymes and drug transporters in response[20–24]. Because of its vital role in detoxification, PXR contains a large, malleable ligand binding pocket that allows its activation by a vast array of small molecules, including PROTACs[18]. Therefore, given the previous challenges encountered in PXR PROTAC design[18,19], in the current work, we tested the concept of PROTAC repurposing to identify PROTACs designed for other targets that may bind and induce degradation of PXR. Through this approach, we found that the murine double minute 2 (MDM2) degrader MD-224[25] potently induced proteasomal degradation of PXR. Surprisingly, however, the degradation activity of MD-224 was either enhanced or blocked by PXR ligands with distinctively different binding modes, and further investigation revealed that MD-224 bound PXR outside the ligand binding pocket at a structural motif that exists in all NRs, although the exact motif sequence and structure vary from receptor to receptor. Accordingly, we found that MD-224 induces the degradation of multiple NRs. Structure- and activity-guided design strategies allowed us to remove MDM2 degradation activity while maintaining degradation of PXR and altering the potency ratios for other NRs. Hence, here we report (1) PROTAC repurposing as a potential route of degrader discovery in certain contexts, (2) semi-rational design of PROTACs to modulate degradation of multiple proteins, and (3) NR targeted degradation through a noncanonical binding site, with the degradation activity potentially tunable bi-directionally with the use of ligands that bind within the ligand binding pocket.

Results

MD-224 induces a rapid loss of PXR protein

We previously designed $CRL4^{CRBN}$-dependent PXR degraders that instead induced degradation of the translation termination factor GSPT1 and resulted in subsequent loss of PXR as a secondary effect[19]. Due to its function as a xenobiotic receptor, PXR has a large spherical ligand-binding pocket that recognizes a vast array of small molecules, so we hypothesized that it may bind to existing PROTACs of various intended targets and that, in some cases, binding would induce PXR's ubiquitination and proteasomal degradation. Using our previously described colorectal SNU-C4 cell line harboring CRISPR/Cas9-mediated HiBiT tagged endogenous PXR ($SNU\text{-}C4^{HiBiT\text{-}PXR}$)[26], we screened a focused library of 45 PROTACs[18] and found that MD-224 reduced HiBiT-PXR signal after 2 h treatment (Fig. 1A and Supplementary Fig. 1). Loss of HiBiT-PXR was maintained for at least 24 h (Fig. 1B) and was confirmed by western blot in SNU-C4 cells containing CRISPR/Cas9-mediated 3xFLAG tagged endogenous PXR ($SNU\text{-}C4^{3xFLAG\text{-}PXR}$) (Fig. 1C). We verified that MD-224 performed its reported role as an MDM2 degrader with minor GSPT1 effect (Fig. 1D), and we found that degradation of both PXR and MDM2 requires the fully intact MD-224 molecule rather than simply the MDM2 ligand (MI-1061), CRBN ligand (lenalidomide, LEN), or the CRBN ligand + linker (lenalidomide-propargyl-C_2-NH_2, LENP) (Fig. 1E-F and Supplementary Data 1). Interestingly, while there was a robust hook effect for MDM2 (dose-dependent protein loss followed by dose-dependent protein increase), loss of PXR protein was complete even at high MD-224 concentrations (Fig. 1C, D, F), suggesting possible diverging mechanisms.

We recently described the design and characterization of a PXR ligand-derived PROTAC, SJYHJ-040, that utilizes the $CRL2^{VHL}$ E3 ubiquitin ligase rather than $CRL4^{CRBN}$ (Fig. 1E and Supplementary Data 1)[27]. In $SNU\text{-}C4^{HiBiT\text{-}PXR}$ cells, MD-224 was more potent and had an earlier time of effect than SJYHJ-040 (Fig. 1G). With 24 h treatment in $SNU\text{-}C4^{3xFLAG\text{-}PXR}$ cells, MD-224 and SJYHJ-040 were equipotent due to SJYHJ-040 showing more pronounced PXR degradation in $SNU\text{-}C4^{3xFLAG\text{-}PXR}$ than in $SNU\text{-}C4^{HiBiT\text{-}PXR}$ (Fig. 1H). This result, which is consistent with our previous findings for SJYHJ-040[27], may indicate clonal variations in E3 expression or activity between the two cell lines. However, the results show that the serendipitously discovered MD-224 is as potent or more so than the designed compound SJYHJ-040 for inducing PXR degradation. The rapid rate of MD-224-induced PXR loss was confirmed in a 293T live-cell kinetic assay, where the full MD-224 effect on PXR level could be achieved in ~30 min (Fig. 1I). PXR was also degraded upon MD-224 treatment of primary human hepatocytes (PHH), showing biological impacts in the natural PXR environment (Supplementary Fig. 2).

MD-224 inhibits PXR function

PXR's most studied function is transcriptional regulation of the CYP3A family of drug metabolism enzymes. The antibiotic rifampicin (RIF) is a prototypical PXR agonist that upregulates *CYP3A4* expression[20,21], and the PXR antagonist SPA70[28] blocks RIF-induced *CYP3A4* expression (Fig. 1J). When $SNU\text{-}C4^{3xFLAG\text{-}PXR}$ cells were co-treated with RIF and MD-224, there was no induction of *CYP3A4* RNA, showing that PXR function was blocked by MD-224 (Fig. 1J). The negative regulation of PXR protein level and activity was not due to inhibition of *PXR* transcription or general transcriptional effects because *PXR* and *GAPDH* RNA were unaffected by MD-224 treatment (Fig. 1J). The results were also not cell line-specific, as MD-224-mediated PXR inhibition was also observed in PHH (Supplementary Fig. 3).

MD-224-induced PXR degradation is CRBN-dependent but MDM2-independent

Because we previously showed that PXR protein loss can occur as an early secondary effect of GSPT1 degradation[19], we next sought to determine if MD-224 directly mediates PXR degradation. MD-224 had minimal activity toward GSPT1 after 2 h treatment (Fig. 1D), indicating that the PXR effect is GSPT1-independent. We generated CRBN knockout 293T cells by CRISPR/Cas9 editing ($293T^{CRBN\ KO}$) (Supplementary Fig. 4) and found that MD-224 only induced HiBiT-PXR degradation when CRBN was restored (Fig. 2A). Furthermore, MD-224 inhibition of PXR activity on a *CYP3A4* promoter reporter was greatly enhanced by introduction of CRBN into $293T^{CRBN\ KO}$ (Fig. 2B). This was unlike the PXR antagonist SPA70, which showed the same inhibition profile in the presence and absence of CRBN (Fig. 2B). Interestingly, MD-224 partially inhibited PXR activity in the absence of CRBN, suggesting that it has an intrinsic antagonistic effect, but this effect was weak compared to PXR degradation (Fig. 2B).

Next, we found that PXR LBD (harboring the ligand binding pocket and adjacent region) is sufficient for degradation by MD-224

https://doi.org/10.1038/s41467-025-64773-5

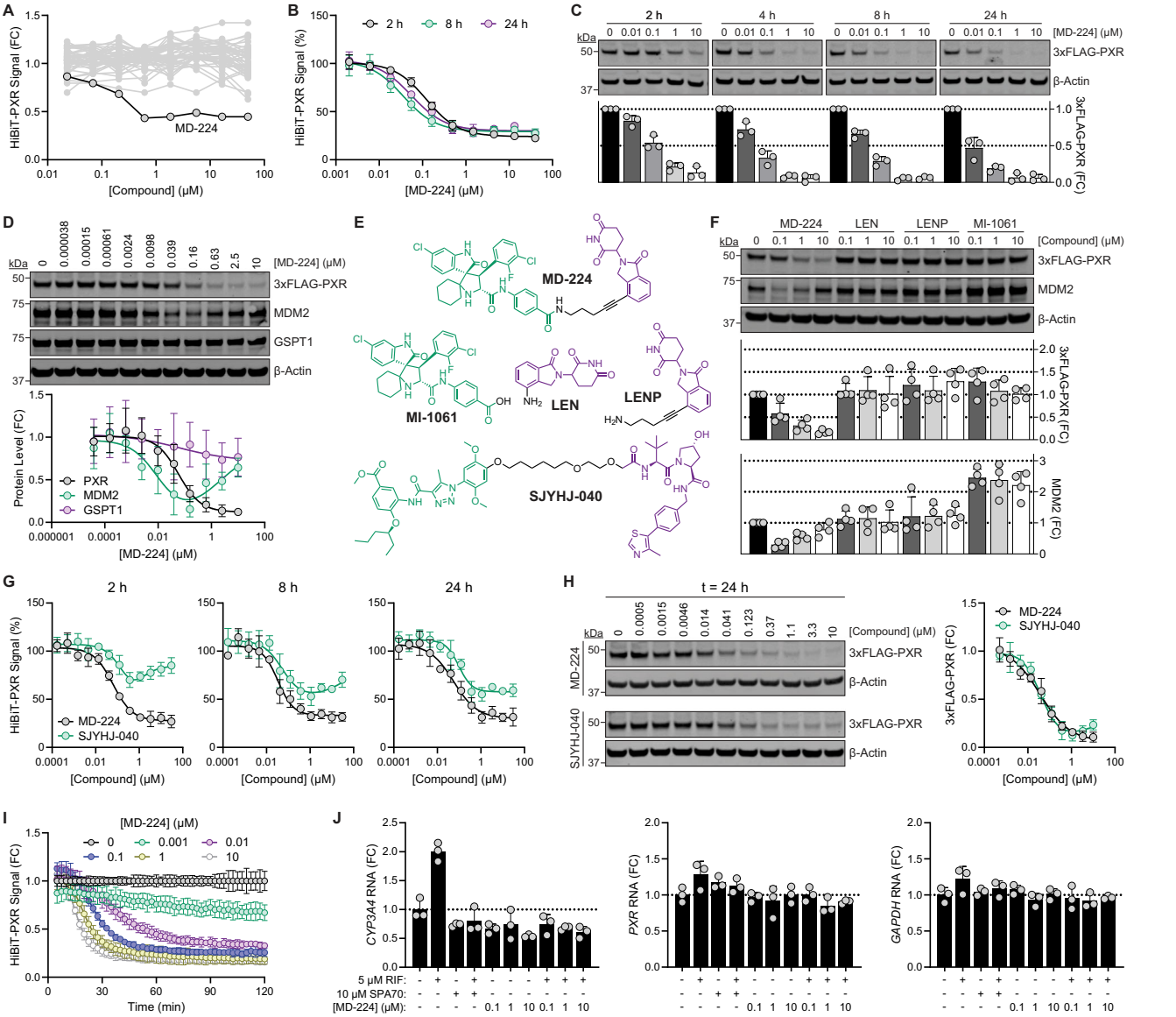

Fig. 1 | MD-224 reduces PXR protein and transcriptional activity. A SNU-C4$^{HiBiT\text{-}PXR}$ cells were treated with PROTACs for 2 h and assessed for HiBiT level ($n = 1$). **B** SNU-C4$^{HiBiT\text{-}PXR}$ cells were treated with MD-224 for the indicated times and assessed for HiBiT level ($n = 6$). **C** SNU-C4$^{3xFLAG\text{-}PXR}$ cells were treated with MD-224 for the indicated times and subjected to western blot using antibodies against FLAG and β-actin. 3xFLAG-PXR was quantified as fold change (FC) relative to the DMSO control at each time point ($n = 3$). **D** SNU-C4$^{3xFLAG\text{-}PXR}$ cells were treated with MD-224 for 2 h and subjected to western blot using antibodies against FLAG, MDM2, GSPT1, and β-actin ($n = 4$). **E** Chemical structures are shown for MD-224, MDM2 ligand MI-1061, CRBN ligand lenalidomide (LEN), CRBN ligand/linker lenalidomide-propargyl-C_2-NH_2 (LENP), and previously designed PXR PROTAC SJYHJ-040. **F** SNU-C4$^{3xFLAG\text{-}PXR}$ cells were treated with the indicated compounds for 2 h and subjected to western blot using antibodies against FLAG, MDM2, and β-actin ($n = 4$). **G** SNU-C4$^{HiBiT\text{-}PXR}$ cells were treated with MD-224 or SJYHJ-040 for 2, 8, or 24 h and assessed for HiBiT level ($n = 4$). **H** SNU-C4$^{3xFLAG\text{-}PXR}$ cells were treated with MD-224 or SJYHJ-040 for 24 h and subjected to western blot using antibodies against FLAG and β-actin ($n = 4$). **I** 293T cells were co-transfected with plasmids encoding HiBiT-PXR, LgBiT, and CRBN. After 48 h, cells were mixed with Vivazine substrate and 0.001-10 μM MD-224, and luminescence was measured every 2.5 min for 2 h ($n = 3$). **J** SNU-C4$^{3xFLAG\text{-}PXR}$ cells were treated with 5 μM PXR agonist rifampicin (RIF), 10 μM PXR antagonist SPA70, or 0.1-10 μM MD-224 as indicated for 24 h. RNA was extracted and subjected to reverse transcription-quantitative polymerase chain reaction (RT-qPCR) to measure expression of *CYP3A4*, *PXR*, or *GAPDH*. Data were normalized to *18S* RNA and represent FC relative to the DMSO control for each gene ($n = 3$). For western blots, one representative blot is shown. Error bars represent mean ± standard deviation (SD) from the stated number (n) of biological replicates. Source data are provided as a Source Data file.

(Supplementary Fig. 5) and that MD-224 induced CRBN interaction with PXR LBD in a cellular NanoBiT assay (Fig. 2C). MD-224 also induced CRBN/DDB1 interaction with PXR LBD in a time-resolved fluorescence energy transfer (TR-FRET) assay with purified proteins (Fig. 2D). However, unlike previous PROTACs that exhibit a sharp bell-shaped curve due to single-protein saturation by the bifunctional molecule, MD-224 showed a broad biphasic curve with only slightly reduced signal at high concentrations, which may be correlated with the lack of hook effect in PXR degradation (Figs. 1, 2D).

Consistent with results from 293T$^{CRBN\ KO}$, in SNU-C4$^{HiBiT\text{-}PXR}$ and SNU-C4$^{3xFLAG\text{-}PXR}$, siRNA-mediated knockdown of CRBN prevented MD-224-induced degradation of both PXR and MDM2 (Fig. 2E, F). Furthermore, MDM2 knockdown did not impact MD-224 activity on PXR, indicating that PXR and MDM2 degradation are independent events (Fig. 2E, F). In addition to CRBN, MD-224 activity required all members of the E3 complex (DDB1, RBX1, and CUL4A/B) as well as ubiquitin (Supplementary Fig. 6). PXR degradation was blocked in the presence of CRBN ligands LEN or LENP, further confirming CRBN dependence

https://doi.org/10.1038/s41467-025-64773-5

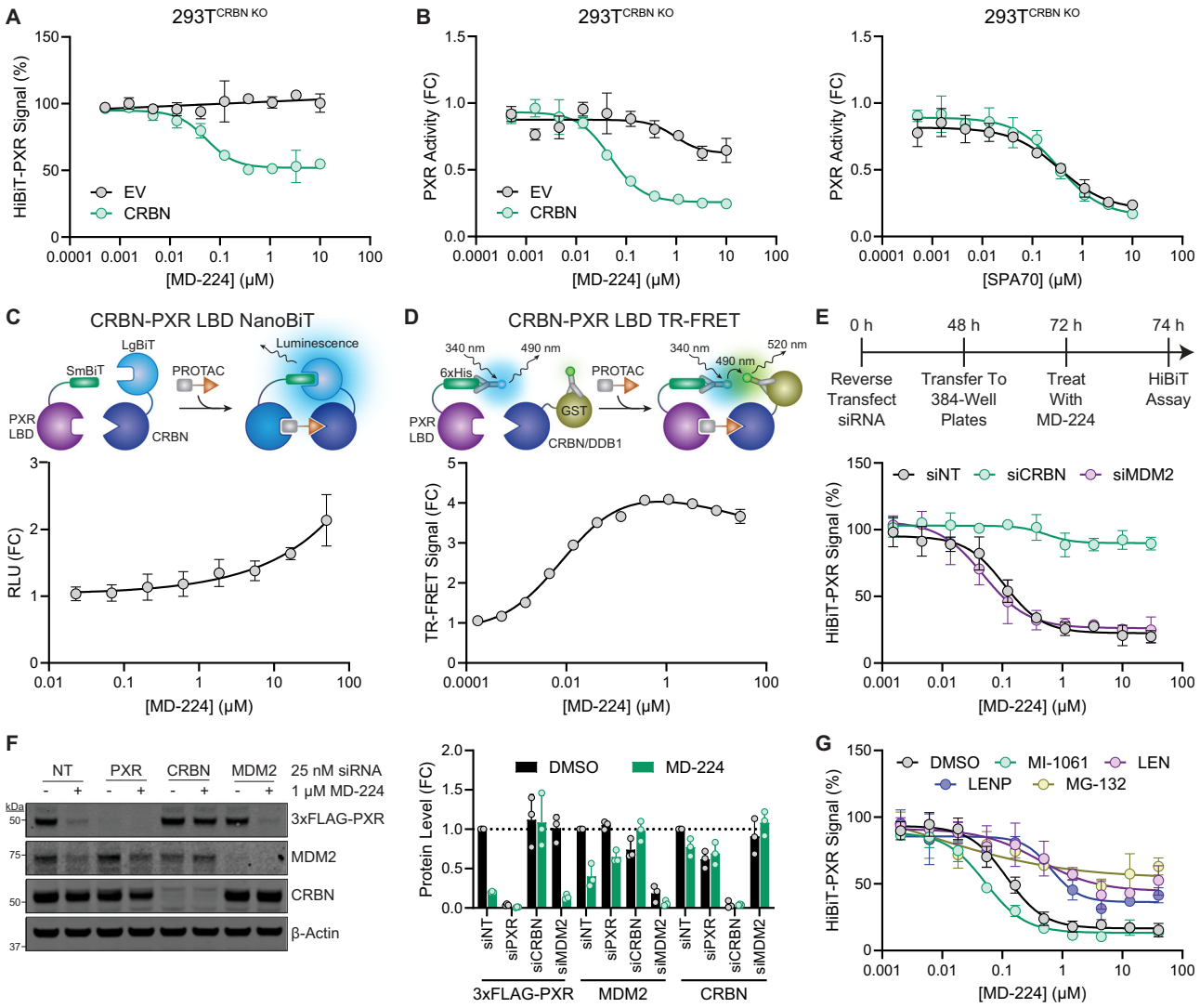

Fig. 2 | MD-224 induces PXR degradation through CRBN recruitment independently of MDM2. A 293T$^{CRBN\ KO}$ cells were co-transfected with a plasmid expressing HiBiT-PXR (20 ng) and either empty vector (EV) or a CRBN-expressing vector (40 ng). After 24 h, cells were treated with the indicated MD-224 concentrations for 2 h and assessed for HiBiT level ($n = 3$). **B** 293T$^{CRBN\ KO}$ cells were co-transfected with a plasmid expressing HiBiT-PXR (20 ng), a plasmid encoding firefly luciferase under the control of a PXR-responsive *CYP3A4* promoter (pGL3-CYP3A4-luc, 1 μg), and either EV or a CRBN-expressing vector (40 ng). After 24 h, cells were treated with the indicated concentrations of MD-224 (left panel) or SPA70 (right panel) in the presence of 5 μM RIF for 24 h and assessed for firefly luciferase activity ($n = 3$). **C** HepG2 cells were co-transfected with plasmids encoding SmBiT-PXR LBD and LgBiT-CRBN. After 48 h, cells were treated with the indicated MD-224 concentrations for 30 min and assessed with the Nano-Glo Live Cell Assay System ($n = 7$). **D** Purified His-PXR LBD and GST-CRBN/DDB1 were mixed with the indicated concentrations of MD-224, incubated for 90 min, and assessed for interaction by TR-FRET ($n = 4$). **E** SNU-C4$^{HiBiT\text{-}PXR}$ cells were transfected with nontargeting control siRNA (siNT) or siRNAs targeting CRBN or MDM2. After 72 h, cells were treated with the indicated MD-224 concentrations for 2 h and assessed for HiBiT level ($n = 4$). **F** SNU-C4$^{3xFLAG\text{-}PXR}$ cells were transfected with the indicated siRNAs. After 72 h, cells were treated with DMSO or 1 μM MD-224 for 2 h and subjected to western blot using antibodies against FLAG, MDM2, CRBN, and β-actin ($n = 3$). One representative blot is shown. **G** SNU-C4$^{HiBiT\text{-}PXR}$ cells were treated for 2 h with the indicated MD-224 concentrations in the presence of DMSO only ($n = 6$) or 10 μM indicated compound ($n = 3$), and HiBiT level was measured. Error bars represent mean ± SD from the stated number (n) of biological replicates. Source data are provided as a Source Data file.

(Fig. 2G). Degradation was also blocked by the proteasome inhibitor MG-132 (Fig. 2G). Together, the data show that MD-224 induces a CRBN-PXR complex, ultimately leading to proteasomal PXR degradation independently of MDM2. The results suggest that the MDM2-binding moiety (MI-1061) may also be the PXR-binding group. Surprisingly, however, co-treatment with MD-224 and MI-1061 did not block PXR degradation; in fact, MI-1061 enhanced MD-224 activity for PXR (Fig. 2G). This result further supports that MD-224 activity for PXR is MDM2-independent, but it introduces a question of how MD-224 interacts with PXR. Specifically, (1) does MD-224 induce PXR degradation through a typical PROTAC mechanism, or is MD-224 a molecular glue that causes CRBN to recognize PXR as a neosubstrate and (2) does MD-224 bind a site other than the ligand binding pocket?

MD-224-mediated PXR degradation is ligand-modulated at alpha helix 12 (α12)

The surprising observation that the MDM2 ligand MI-1061, which constitutes the probable PXR-binding moiety of MD-224, did not block PXR degradation prompted us to test the effects of known PXR ligands on MD-224 activity. We co-treated SNU-C4$^{HiBiT\text{-}PXR}$ and SNU-C4$^{3xFLAG\text{-}PXR}$ cells with MD-224 and a panel of PXR agonists (SR12813, T0901317, SJB7, and SJPYT-328) or antagonists (SPA70 and SJPYT-331) (Fig. 3A, B). For comparison, we conducted the same competition experiment with the PXR PROTAC SJYHJ-040, whose degradation activity was blocked by all ligands (Fig. 3A). Interestingly, there was a range of co-treatment effects on MD-224 degradation activity, including enhancement (SR12813 and T0901317), weak blockage (SJB7), and strong blockage

https://doi.org/10.1038/s41467-025-64773-5

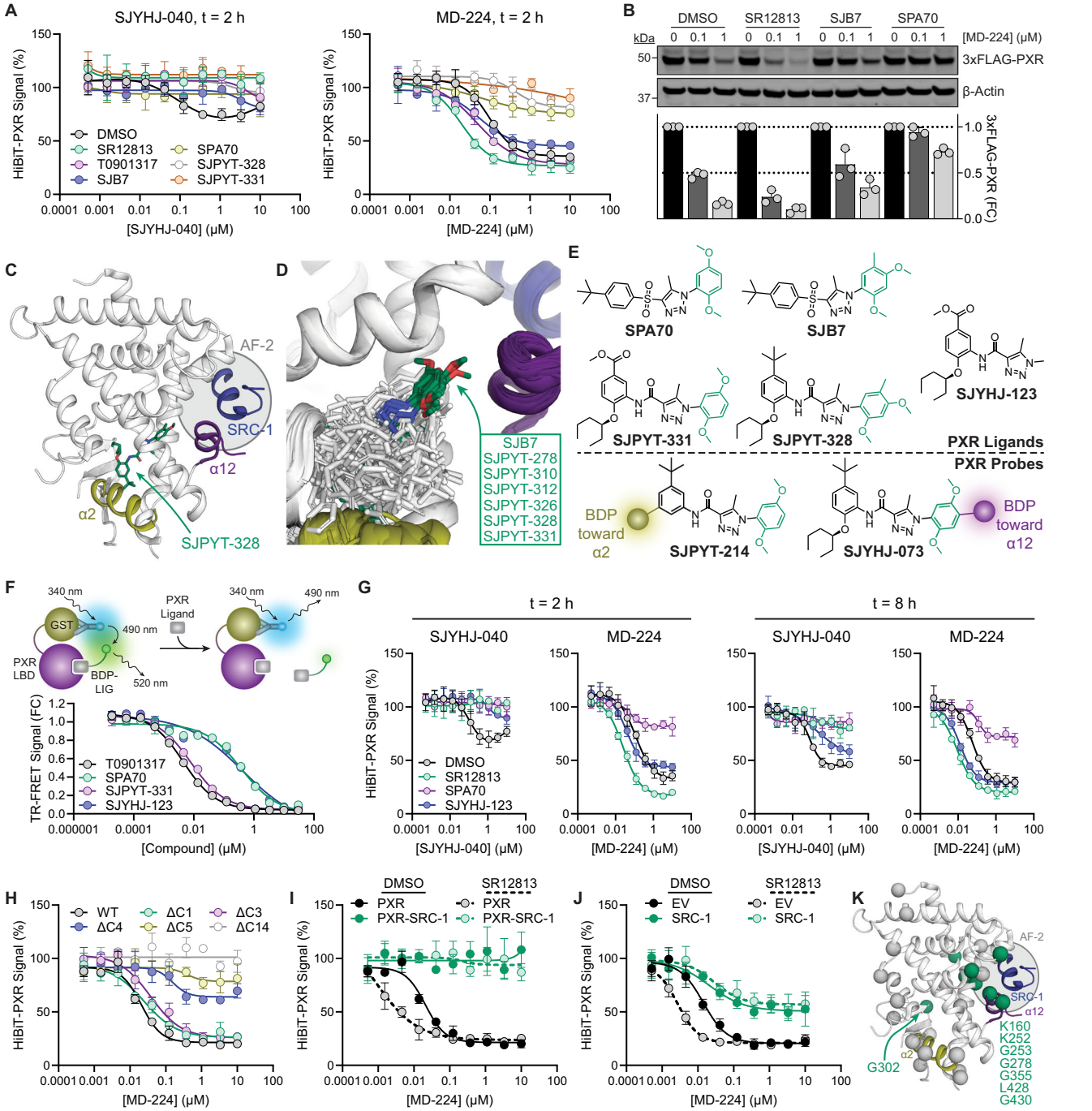

Fig. 3 | MD-224 does not occupy the PXR ligand binding pocket. A SNU-C4$^{HiBiT\text{-}PXR}$ cells line were treated for 2 h with SJYHJ-040 or MD-224 +/− 10 μM PXR ligand, and HiBiT level was measured ($n = 3$). **B** SNU-C4$^{3xFLAG\text{-}PXR}$ cells were treated for 2 h with MD-224 +/− 10 μM PXR ligand, and western blot was performed ($n = 3$). One representative blot is shown. **C** The crystal structure of PXR LBD bound to SJPYT-328 is shown (PDB 8SVS). **D** All PXR LBD crystal structures are overlaid ($n = 65$) with ligands as sticks. SJB7 and analogs are colored green. **E** Chemical structures of the first-generation PXR antagonist (SPA70) and agonist (SJB7), and the second-generation antagonist (SJPYT-331) and agonist (SJPYT-328) are shown. The green-highlighted ring was omitted from SJPYT-331 to make SJYHJ-123. Partial chemical structures of fluorescent PXR probes are also shown. **F** PXR LBD binding was assessed by TR-FRET assay measuring displacement of a PXR ligand with a fluorophore directed at PXR's α2 (SJPYT-214, α2 probe, $n = 3$). **G** SNU-C4$^{HiBiT\text{-}PXR}$ cells were treated for 2 h or 8 h with SJYHJ-040 or MD-224 +/− 10 μM PXR ligand, and HiBiT level was measured ($n = 4$). **H** 293T cells transfected with plasmids encoding HiBiT-tagged wild-type (WT, residues 1-434) or C-terminally truncated (e.g., ΔC1 is residues 1-433) PXR were treated with MD-224 for 2 h and assessed for HiBiT level ($n = 3$). **I** 293T cells transfected with plasmids encoding HiBiT-tagged WT PXR or PXR with C-terminally fused 23-amino acid SRC-1 peptide (residues 678-700, PXR-SRC-1) were treated for 2 h with MD-224 +/− 10 μM SR12813 and assessed for HiBiT level ($n = 3$). **J** 293T cells transfected with a plasmid expressing HiBiT-PXR (20 ng) +/− a vector expressing SRC-1 residues 621-765 (2 μg) were treated for 2 h with MD-224 +/− 10 μM SR12813 and assessed for HiBiT level ($n = 4$). **K** PXR LBD structure is shown (PDB 8SVS); Cα of all tested mutations are shown as spheres, and mutations that reduce MD-224-mediated degradation are colored green. Error bars represent mean ± SD from the stated number (n) of biological replicates. Source data are provided as a Source Data file.

(SPA70, SJPYT-328, and SJPYT-331), indicating that unlike SJYHJ-040, MD-224 does not bind within the ligand binding pocket of PXR.

To investigate potential differences among PXR ligands, we examined all ligand-bound PXR LBD structures deposited in the PDB (Fig. 3C-D, Supplementary Data 2). Ligands that blocked MD-224 activity (SJB7, SJPYT-328, SJPYT-331, and related analogs) were clear outliers in binding mode, as they project toward the top of α12 in the direction of the coactivator SRC-1 binding surface [known as the activation function-2 (AF-2) surface]. Although no crystal structure of SPA70 is available, its high similarity to SJB7 suggests that it likely binds like SJB7 (Fig. 3E and Supplementary Data 1). The compounds that enhance MD-224 activity (T0901317 and SR12813) bind deep within the pocket away from α12, and SR12813 has been shown to bind in multiple modes, one of which is stabilized by SRC-1 binding (Supplementary Fig. 7)[29,30]. Therefore, MD-224 may bind proximally to the ligand binding pocket, possibly in the SRC-1 peptide binding site, and its activity may be blocked by compounds that bind near α12 or that cause α12 displacement, as we previously described for SPA70[31]. Because SR12813 does not extend over α12 and is mobile within the pocket, it may adopt a binding mode that acts synergistically with MD-224 to enhance PXR degradation.

To test if ligand proximity to α12 indeed impacts MD-224 co-treatment outcome, we synthesized SJYHJ-123, which lacks the α12-interacting ring of SJPYT-331 (Fig. 3E and Supplementary Data 1). Using a TR-FRET assay that measures displacement of a fluorophore-linked PXR ligand (SJPYT-214)[27] from the PXR ligand binding pocket, we found that SJYHJ-123 binds PXR LBD with affinity equal to SPA70 (Fig. 3E, F and Supplementary Data 1). In SNU-C4$^{HiBiT\text{-}PXR}$ cells, SJYHJ-123 blocked SJYHJ-040-mediated PXR degradation but enhanced MD-224-mediated degradation, further reinforcing that MD-224 does not bind within the canonical pocket but may rely on α12 (Fig. 3G). Because α12 resides on PXR's C-terminus, we generated C-terminal HiBiT-PXR truncations to directly test α12 influence on MD-224 activity. Serial deletions of 1, 3, 4, or 5 residues or the entire α12 (ΔC14) resulted in a stepwise loss of MD-224 degradation function (Fig. 3H). Furthermore, addition of a 23-amino acid coactivator peptide to PXR's C-terminus (PXR-SRC-1) fully ablated MD-224 activity, and the activity could not be enhanced by co-treatment with SR12813 (Fig. 3I). Co-expression of unfused SRC-1 NR interaction domain also reduced MD-224 activity and prevented enhancement by SR12813 (Fig. 3J, Supplementary Fig. 8).

With few reported exceptions[32], CRBN-dependent molecular glues largely act on neosubstrates with a β-hairpin and a glycine at a key position that facilitates recognition by CRBN, but PROTACs do not have such a preference. Molecular glues also do not encounter hook effects while PROTACs may or may not experience such effects, depending on complex factors. Our observations that MD-224 had a hook effect for MDM2 but not PXR and that the PXR PROTAC SJYHJ-040 showed a hook effect for PXR (Fig. 1) led us to question whether MD-224 may be a molecular glue degrader for PXR. We individually mutated PXR's 27 glycine residues to alanine and identified five mutants (G253A, G278A, G302A, G355A, and G430A) that reduced MD-224 activity (Supplementary Fig. 9). However, degradation of all five was at least partially rescued by SR12813 co-treatment (Supplementary Fig. 9); therefore, MD-224 is likely not a molecular glue degrader of PXR, although a noncanonical recognition motif could conceivably mediate the CRBN-PXR interaction[32]. Next, to find lysine residues that may be ubiquitinated by the induced PXR-E3-E2 complex, we mutated the 15 lysine residues in PXR LBD to arginine and identified two mutants (K160R and K252R) with reduced MD-224 sensitivity (Supplementary Fig. 10A). Both mutants were highly resistant to degradation even in the presence of SR12813 (Supplementary Fig. 10B, C). Interestingly, when the locations of all glycine and lysine residues of consequence were analyzed, other than G302 which resides in a β-hairpin region proximal to residues critical for PXR structure and ligand binding, all responsive positions clustered around α12 and the AF-2 surface (Fig. 3K). Together, the ligand competition, mutagenesis, and SRC-1 competition results suggested that the AF-2 surface is a key component of MD-224-induced PXR degradation. In support of this, a triple mutant PXR (S208W, S247W, C284W) that is incapable of binding ligands within the ligand binding pocket[31,33] was susceptible to MD-224-mediated degradation while no longer responding to SJYHJ-040 treatment (Supplementary Fig. 11). Conversely, a single α12 mutation (L428Y) that retains ligand-modulated activity[34] rendered PXR resistant to MD-224 but not SJYHJ-040 (Supplementary Fig. 11), thus differentiating the binding modes of the two degraders.

To differentiate between a PROTAC (in which the two ends of the degrader molecule bind the E3 ligase and target protein independently) and a molecular glue mechanism (in which the degrader molecule only binds the E3 ligase, changing its substrate specificity), we performed surface plasmon resonance (SPR) with PXR LBD (Supplementary Fig. 12). We found that MD-224 does indeed bind PXR LBD and that the noncompetitive PXR ligand T0901317 does not alter MD-224 binding affinity for PXR LBD. We also confirmed the PXR LBD-MD-224-CRBN ternary complex and that T0901317 does not inhibit complex formation. Thus, MD-224 appears to act as a bona fide PXR PROTAC by binding to a site other than the classical ligand binding pocket.

MD-224 induces degradation of multiple NRs

Because we found that MD-224 degrades a protein (PXR) other than its originally intended target (MDM2), we sought to test the overall specificity of this PROTAC by whole-proteome profiling. We have previously reported failures to detect PXR using tandem mass tag mass spectrometry (TMT-MS) in parental SNU-C4 and SNU-C4$^{3xFLAG\text{-}PXR}$ cells, which both highly express PXR[19,27]. Therefore, we tested 293T cells overexpressing PXR to the same relatively low level as the HiBiT-PXR experiments performed in 293T to this point. TMT-MS found a reduction of endogenous MDM2 by both 100 nM and 1 μM MD-224, but was still not able to detect PXR protein (Fig. 4A-B and Supplementary Data 3-4). Indeed, this is a general proteomic sensitivity issue, as data-independent acquisition (DIA) MS was also not able to detect PXR protein in SNU-C4$^{3xFLAG\text{-}PXR}$ cells (Supplementary Data 5); however, PXR detection by DIA-MS was achieved once 3xFLAG-PXR was immunoprecipitated from the same cells (Supplementary Data 6). We then performed DIA-MS in 293T with increased PXR plasmid amount, which allowed us to observe PXR protein and its expected reduction with 100 nM and 1 μM MD-224 (Fig. 4C-D, Supplementary Data 7, 8); however, MDM2 was unobservable in these datasets. Furthermore, while MD-224 appears to be a clean PROTAC overall with regards to observed off-targets, different off-targets were found by TMT and DIA methods, indicating that caution should be taken when drawing conclusions from such experiments.

In PXR, the AF-2 surface is required for MD-224-mediated degradation, and MD-224 does not appear to bind within the canonical ligand binding pocket (Fig. 3). The AF-2 surface is a structural feature shared by NRs, although the primary sequences vary and α12 and the AF-2 region are known to be flexible (Fig. 4E, F and Supplementary Fig. 13). Therefore, we assessed additional NRs for MD-224 sensitivity and found that three other members of the NR1 subfamily (CAR, LXRα, and LXRβ) were degraded (Fig. 4G). The final two NR1 members VDR and FXR were unaffected, and additional NRs, including mouse PXR (mPXR), ERα, and AR, were either unaffected or even stabilized. Secondary structure analysis of sensitive NR1 LBDs (PXR, CAR, LXRα, and LXRβ) and insensitive NR1 LBDs (VDR and FXR) showed no correlation between structure and degradation (Fig. 4E), but because single mutations on PXR's AF-2 affect MD-224 activity, the NR-PROTAC interaction and resulting NR-PROTAC-E3-E2 complex may be sensitive to specific residue differences. In support of this, degradation of both LXRα and LXRβ was fully blocked by all tested LXR ligands, indicating

https://doi.org/10.1038/s41467-025-64773-5

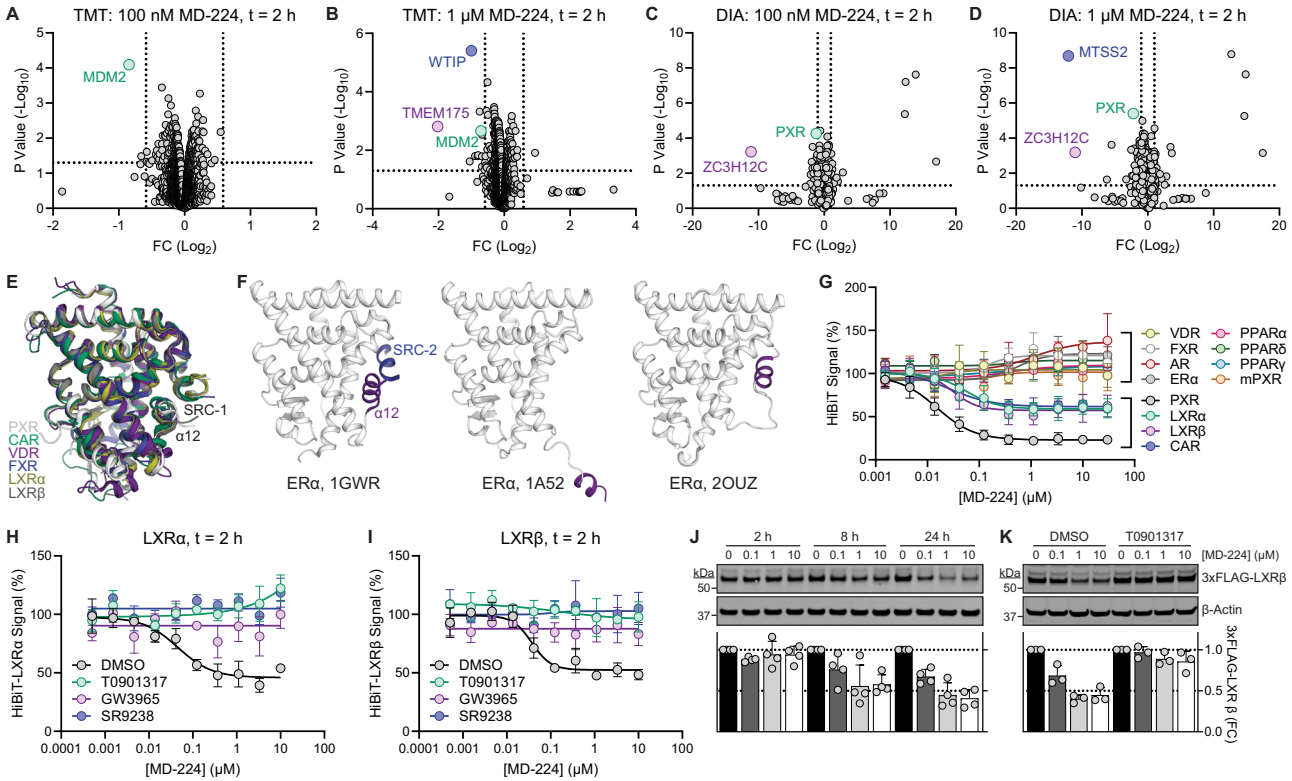

Fig. 4 | MD-224 induces degradation of additional NRs. A, **B** 293T cells transfected with pcDNA3-FLAG-PXR (120 ng/10 cm dish) were treated with DMSO, 100 nM MD-224, or 1 μM MD-224 for 2 h and analyzed by TMT-MS ($n = 2$ for each treatment). Plots compare MD-224 *vs.* DMSO with vertical lines at absolute FC = 1.5 and horizontal line at $P = 0.05$. One-way ANOVA was used to identify differential expression events, and P values were corrected for multiple testing using the Benjamini-Hochberg method. **C**, **D** 293T cells transfected with pcDNA3-FLAG-PXR (250 ng/well in six-well plates) were treated with DMSO, 100 nM MD-224, or 1 μM MD-224 for 2 h ($n = 3$ for each treatment), and analyzed by DIA. Plots compare MD-224 *vs.* DMSO with vertical lines at absolute FC = 2 and horizontal line at $P = 0.05$. Two-sided tests were used, and P values were adjusted for multiple comparisons using the Benjamini–Hochberg method. **E** LBD crystal structures of PXR (PDB 8SVS), CAR (PDB 1XVP), VDR (PDB 1S0Z), FXR (PDB 3FXV), LXRα (PDB 3IPQ), and LXRβ (PDB 1P8D) are overlaid. SRC-1 is shown for structures containing the peptide. **F** Crystal structures of ERα LBD bound to estradiol and coactivator SRC-2 peptide (PDB 1GWR), estradiol alone (PDB 1A52), and the selective estrogen receptor modulator lasofoxifene alone (PDB 2OUZ) are shown. **G** 293T cells transfected with plasmids expressing HiBiT-tagged NRs were treated with MD-224 for 2 h and assessed for HiBiT level [$n = 4$ for all NRs except PXR ($n = 40$), and LXRα, LXRβ, and CAR ($n = 8$)]. **H** 293T cells transfected with a plasmid encoding HiBiT-tagged LXRα were treated for 2 h with MD-224 +/− 10 μM indicated LXR ligand and assessed for HiBiT level ($n = 3$). **I** 293T cells were treated as in (**H**) but using HiBiT-LXRβ ($n = 3$). **J** SNU-C4$^{3xFLAG\text{-}LXR\beta}$ cells were treated with MD-224 for the indicated times and subjected to western blot ($n = 4$). **K** SNU-C4$^{3xFLAG\text{-}LXR\beta}$ cells were treated for 24 h with MD-224 +/− 10 μM T0901317, and western blot was performed ($n = 3$). For western blots, one representative blot is shown. Error bars represent mean ± SD from the stated number (n) of biological replicates. Source data are provided as a Source Data file.

differences in the degradation mechanisms of PXR versus LXRs (Fig. 4H–K and Supplementary Data 1).

Structure-guided synthesis of NR-selective MD-224 derivatives

To validate the PROTAC repurposing approach, we sought to study the structure-activity relationship among MD-224 analogs and degradation of MDM2 versus our model NR, PXR. MDM2 degradation has been extensively studied[25,35], and certain analogs are commercially available including MD-222 (equipotent to MD-224 for MDM2 degradation) and MG-277 (a molecular glue degrader of GSPT1) (Fig. 5A and Supplementary Data 1). Surprisingly, changing the alkyne in the MD-224 linker to an alkane (MD-222) fully removed all PXR activity (Fig. 5B), suggesting that PXR may have strict requirements for PXR-degrader-E3 geometry. MG-277 is further modified by the removal of the benzamide from the MDM2-binding moiety, resulting in a very slight PXR reduction that was likely a consequence of potent GSPT1 degradation by this compound. We altered the benzamide of MD-224 by replacing the benzene ring with bicyclo[2.2.2]octane (SJYHJ-048), and this change enhanced PXR degradation activity without significantly affecting MDM2 degradation activity (Fig. 5A-B and Supplementary Data 1). Alkylation of the MDM2 ligand (SJYHJ-059) resulted in complete loss of MDM2 activity, as we expected based on the crystal structure of MDM2 with the MI-1061 analog SAR405838 (Supplementary Fig. 14)[36]. However, this modification also resulted in partial loss of PXR activity and a gain of GSPT1 activity. To remove GSPT1 activity, we used a "degron blocking" strategy wherein a methoxy group was appended to the CRBN ligand to prevent binding of the neosubstrate β-hairpin degron (SJYHJ-108)[37]. The resulting compound SJYHJ-108 had enhanced PXR activity compared to SJYHJ-059 and was inactive for both MDM2 and GSPT1 (Fig. 5A-B and Supplementary Data 1). Thus, we were able to successfully modify an MDM2 degrader to remove MDM2 degradation but maintain PXR degradation.

We next characterized the analogs with a panel of TR-FRET assays that measured CRBN binding (Fig. 5C), MDM2 binding (Fig. 5D), CRBN-MDM2 complex formation (Fig. 5E), CRBN-PXR LBD complex formation (Fig. 5F), and PXR LBD binding (Fig. 5G, H). All compounds bound CRBN with high affinity, with SJYHJ-048 and the degron-blocked SJYHJ-108 being the most potent (Fig. 5C). As intended, the alkylated SJYHJ-059 and SJYHJ-108 lost nearly all observable MDM2 binding (Fig. 5D) and failed to induce CRBN-MDM2 interaction (Fig. 5E), consistent with lack of MDM2 degradation (Fig. 5B). The CRBN-MDM2 complex assay showed the classical PROTAC bell-shaped curves, unlike the broad curves observed with CRBN-PXR LBD (Figs. 2D, 5F), indicating possible mechanistic differences in complex formation. The potency and

https://doi.org/10.1038/s41467-025-64773-5

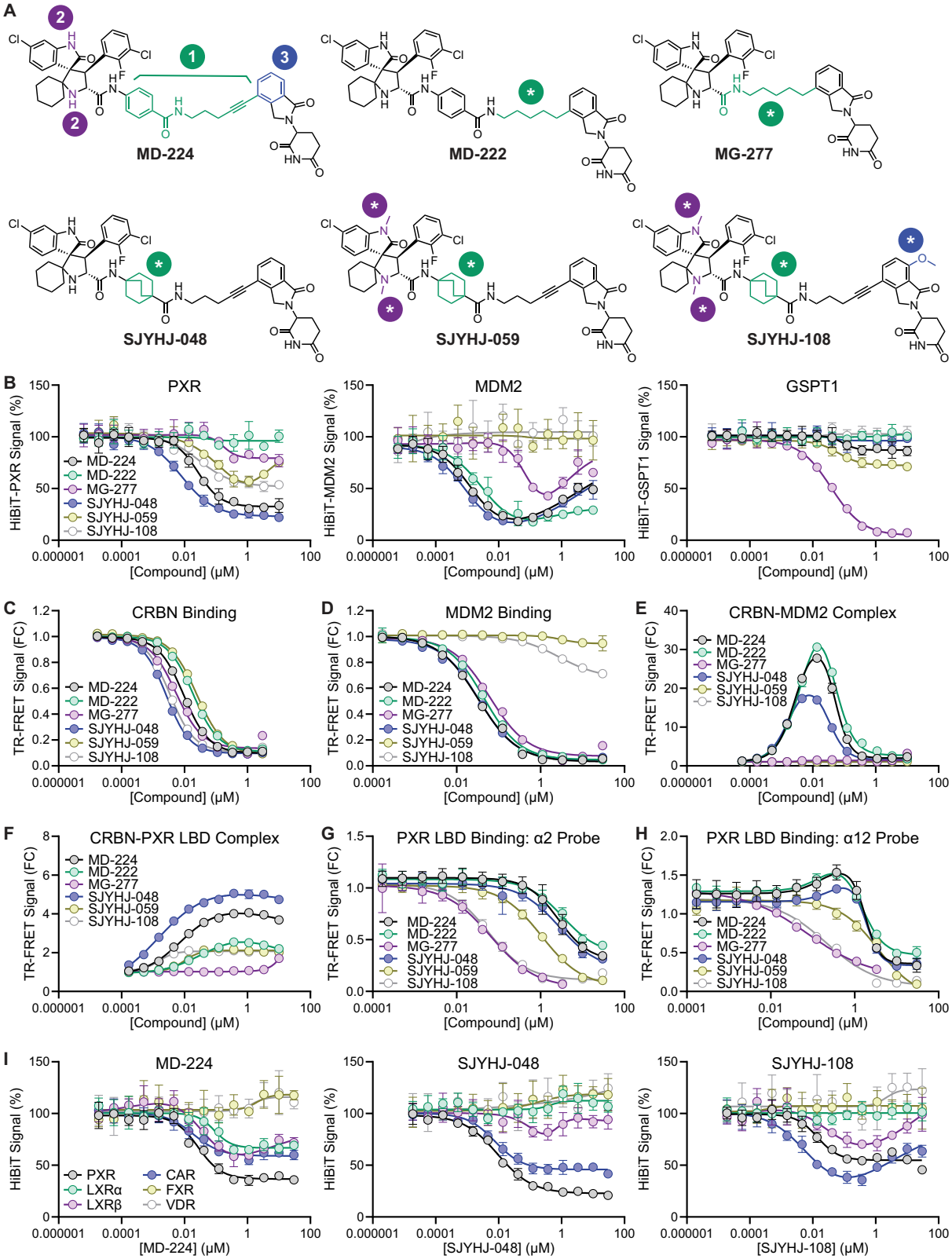

extent of CRBN-PXR LBD complex correlated with the PXR degradation activity (SJYHJ-048 > MD-224 > SJYHJ-108 > SJYHJ-059), with the exception of MD-222, which induced a low-level complex without degradation (Fig. 5F).

For PXR LBD binding, we utilized two fluorescent probes with distinct fluorophore orientations and assessed the abilities of MD-224 analogs to compete with probe binding[27]. In the first probe (SJPYT-214), the fluorophore is oriented toward α2 (Fig. 3C, E and Supplementary Data 1). There was no correlation between PXR degradation potency and ability to compete with the α2 probe for PXR LBD binding, as the two most potent PXR degraders (SJYHJ-048 and MD-224) and the non-degrader MD-222 had equally weak α2 competing activity (Fig. 5G). The trend was the same for competitive binding of the second probe (SJYHJ-073), which has the fluorophore oriented toward α12

https://doi.org/10.1038/s41467-025-64773-5

Fig. 5 | Rational design of NR-selective degraders. A The chemical structures of commercially available (MD-222 and MG-277) and in-house (SJYHJ-048, -059, and -108) MD-224 analogs are shown. The modified areas are (1) green, linker, (2) purple, MDM2 ligand, and (3) blue, CRBN ligand. **B** 293T cells were transfected with plasmids expressing HiBiT-tagged PXR (left panel), MDM2 (middle panel), or GSPT1 (right panel). After 48 h, cells were treated with the indicated compound concentrations for 2 h and assessed for HiBiT level ($n = 4$). **C** CRBN binding affinity of the indicated compounds was assessed by a TR-FRET assay that measures displacement of a fluorescently labeled CRBN ligand ($n = 4$). **D** MDM2 binding affinity of the indicated compounds was assessed by a TR-FRET assay that measures displacement of a fluorescently labeled MDM2 substrate peptide ($n = 4$). **E** Purified GST-MDM2 and His-CRBN/DDB1 were mixed with the indicated compounds and assessed for interaction by TR-FRET ($n = 4$). **F** Purified His-PXR LBD and GST-CRBN/DDB1 were mixed with the indicated compounds and assessed for interaction by TR-FRET ($n = 4$). **G** PXR LBD binding affinity of the indicated compounds was assessed by a TR-FRET assay that measures displacement of a PXR ligand with a fluorophore directed at the α2 region of the protein (SJPYT-214, α2 probe, $n = 4$). **H** PXR LBD binding affinity of the indicated compounds was assessed by a TR-FRET assay that measures displacement of a PXR ligand with a fluorophore directed at the α12 region of the protein (SJYHJ-073, α12 probe, $n = 4$). **I** 293T cells were transfected with plasmids expressing HiBiT-tagged NRs. After 48 h, cells were treated with MD-224 (left panel), SJYHJ-048 (middle panel), or SJYHJ-108 (right panel) for 2 h and assessed for HiBiT level ($n = 4$). Error bars represent mean ± SD from the stated number (n) of biological replicates. Source data are provided as a Source Data file.

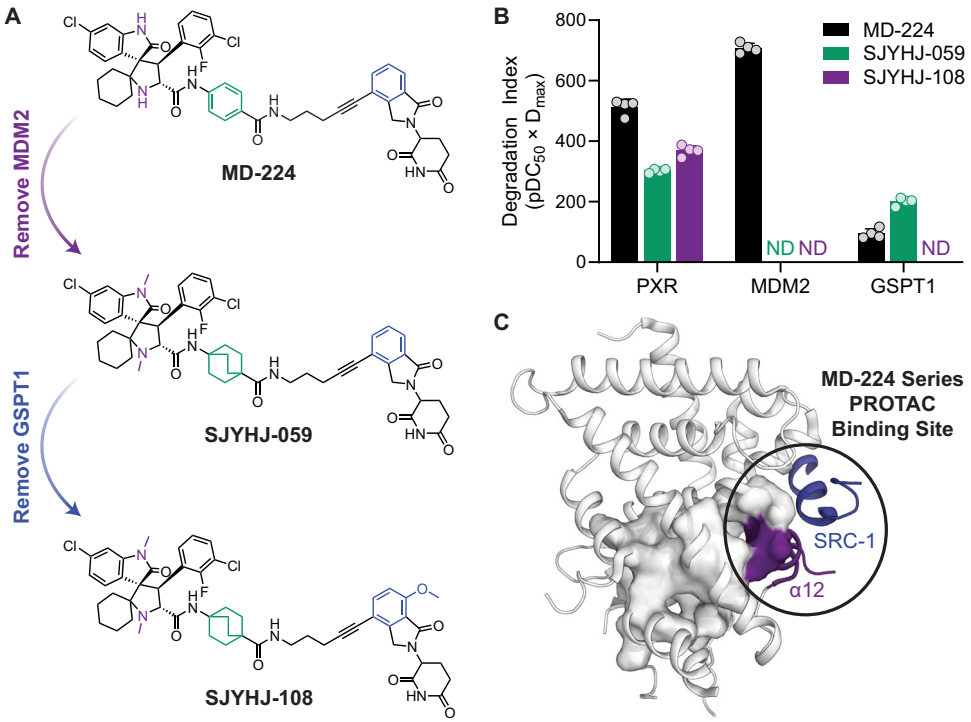

Fig. 6 | Summary of key MD-224 series PROTAC parameters. A The MDM2 ligand of MD-224 was alkylated to remove MDM2 degradation (purple). Then, a methoxy was added to the CRBN ligand to remove GSPT1 activity (blue). An additional substitution in the MDM2 ligand/linker region enhanced PXR degradation (green). **B** To visualize both potency and maximal degradation, a degradation index was generated by converting DC_{50} to pDC_{50} (negative log of DC_{50} in molar) and multiplying by D_{max} for each compound ($n = 4$ biological replicates, error bars represent mean ± SD). ND, not determined; a degradation index could not be calculated because there was no observable degradation. **C** The crystal structure of PXR LBD (PDB 8SVS) is shown with residues within 5 Å of the bound ligand (SJPYT-328) displayed as a surface view. The proposed binding site of MD-224 and analogs is circled. Source data are provided as a Source Data file.

(Fig. 3C, E, Fig. 5H, and Supplementary Data 1). However, competition of the α12 probe showed a biphasic curve in which SJYHJ-048, MD-224, and MD-222 first stabilized the probe-PXR LBD interaction before competing. These results reinforce the idea that MD-224 and its derivatives bind the AF-2 surface rather than within the pocket. Indeed, binding within the canonical binding pocket appears to be detrimental to degradation activity, as compounds with higher apparent affinities had lower degradation efficiencies. These results together with our observation that the MDM2-binding moiety alone (MI-1061) does not block PXR degradation (Fig. 2G) also suggest that analogs or truncated compounds may bind PXR in different conformations with altered binding affinities and/or degradation efficiencies, possibly due to compound-specific preferences in binding more toward the ligand binding pocket or more outward toward the AF-2 surface.

After characterizing the analog activities toward the main proteins of study, we wished to assess their differential NR activities. The parental MD-224 induced degradation of PXR > CAR = LXRα = LXRβ (Figs. 4G and 5I). SJYHJ-048 gained potency for both PXR and CAR, lost LXRα activity, and had reduced LXRβ degradation (Fig. 5I). Interestingly, SJYHJ-108 had an altered degradation profile (CAR > PXR > LXRβ) due to a further gain of CAR degradation, slight gain of LXRβ activity, and partial loss of PXR degradation. These results demonstrate that activity-guided structure-activity relationships can be conducted to alter the balance of NRs degraded by MD-224 derivatives at a non-canonical small molecule binding site. A summary of the structure-activity relationship related to the representative NR PXR is presented in Fig. 6.

Discussion

Although dedicated LBDs make NRs more readily druggable compared to other transcription factors, the majority of NRs remain clinically untargeted due largely to nonspecific ligands. This polypharmacology

is evident in our current study, as T0901317 was used as an agonist for PXR, LXRα, and LXRβ and is known to modulate other receptors[38]. Such effects are difficult to avoid because the primarily hydrophobic ligand-binding pockets interact with diverse lipophilic ligands. The AF-2 surface presents an alternative site that may be targeted, and though the site has been purported to interact with certain ligands that may act as antagonists, such effects remain unexplored[39]. We show here that PROTACs induce NR degradation by binding to the AF-2 surface and do so more effectively than PROTACs designed to bind within the ligand binding pocket, in line with our previous proposal that surface clefts may be simpler than buried pockets to target with PROTACs due to immediate solvent access by the E3 ligand[18]. We also discovered that the degradation activity of the AF-2-targeting PROTAC can be either enhanced or reduced by binders of the canonical binding pocket with different binding modes. It may even be intuitive that this would occur, as NR ligands are known to induce conformational changes at the AF-2 surface, particularly in cases of agonists versus antagonists[31,40] or when ligands extend toward α12[34]. This tunable property of a PROTAC has not been previously reported and demonstrates a potential avenue to further control protein degradation through ligand-gated PROTAC activity.

While molecular glues must be discovered serendipitously and have no relation to ligands of the degraded protein target, PROTACs are designed molecules consisting of a ligand for the protein of interest, a linker, and a ligand for an E3 ubiquitin ligase of interest. PROTAC repurposing represents a hybrid approach, whereby a degrader is discovered from a library of existing PROTACs, and specific activities are then dialed in or out by structure- and activity-guided design. Previous studies have been conducted with groups of related proteins and nonspecific target ligands (e.g., kinases[41] or bromodomain-containing proteins[42]), but here we discovered a PROTAC (MD-224) that degrades a select set of proteins (NRs) unrelated to the originally designed target (MDM2). We then used rational design strategies to remove activities toward MDM2 and the commonly observed molecular glue target GSPT1. These findings set the stage for further optimization of PROTAC derivatives with altered NR degradation profiles.

PROTAC selectivity is generally thought of in terms of the number of proteins degraded by the molecule, but we previously showed that multiple PROTACs can activate, rather than degrade, the NR PXR[18]. Therefore, particularly in cases where a promiscuous ligand is the nucleation point for a PROTAC, it can be reasonably speculated that the PROTAC may bind and inhibit or activate multiple proteins, although degradation is only observed for a subset of those proteins. Hence, in our efforts, we sought to fully ablate MDM2 binding in addition to removing MDM2 degradation activity by the MD-224 derivatives. However, although polypharmacology is often viewed as detrimental to drugs, it may be beneficial in certain scenarios. MD-224, for example, may serve as a potent anticancer agent through MDM2 degradation while mitigating metabolism-related events by degrading NRs involved in transcription of drug metabolism genes (PXR, CAR, LXRα, and LXRβ). As with monovalent inhibitors, the benefits and drawbacks of each PROTAC should be considered in context-specific manners, and our work has established PROTAC repurposing as a potential method to discover and design PROTACs for use in certain contexts.

Methods

Cell culture

SNU-C4 cells were obtained from the Korean Cell Line Bank (KCLB, cat. # 0000C4). SNU-C4$^{HiBiT\text{-}PXR}$ and SNU-C4$^{3xFLAG\text{-}PXR}$ cells containing either a HiBiT or 3xFLAG tag fused to the N-terminus of endogenous PXR were generated using CRISPR/Cas9 technology and have been described[19,26]. Parental SNU-C4 and the CRISPR/Cas9 derivatives were maintained in RPMI-1640 medium (ATCC, cat. # 30-2001) with 10% fetal bovine serum (FBS, Cytiva, cat. # SH30396.03) and 1X penicillin/streptomycin (pen/strep, Thermo Fisher Scientific, cat. # 15140122). HepG2/C3A cells were obtained from the American Type Culture Collection (ATCC, cat. # CRL-3581) and maintained in Eagle's Minimum Essential Medium (EMEM, ATCC, cat. # 30–2003) with 10% FBS and 1X pen/strep. 293T/17 cells were obtained from ATCC (cat. # CRL-11268) and maintained in Dulbecco's Modified Eagle Medium (DMEM, ATCC, cat. # 30-2002) with 10% FBS and 1X pen/strep. PHH were obtained through the Human Hepatocyte Isolation Distribution (University of Pittsburgh), part of the Pittsburgh Liver Research Center Clinical Biospecimen Repository and Processing Core, Pittsburgh, Pennsylvania, which was funded by grant P30DK120531, now called the Human Liver Tissue and Hepatocyte Research Resource funded by grant R24DK139775. The case numbers for PHH donors 1-3 were 22-007, 22-009, and 23-001-04, respectively. PHH were maintained in Williams' Medium E (MilliporeSigma, cat. # W1878-500ML) supplemented with Primary Hepatocyte Maintenance Supplement (Thermo Fisher Scientific, cat. # CM4000). Cells were incubated in a humidified atmosphere at 37 °C with 5% CO_2, authenticated by short tandem repeat (STR) DNA profiling at the St. Jude Hartwell Center for Biotechnology, and routinely verified to be mycoplasma free by using the MycoProbe Mycoplasma Detection Kit (R&D Systems, cat. # CUL001B). Cell counts were obtained with a Countess II Automated Cell Counter (Thermo Fisher Scientific) using trypan blue staining. For selected experiments performed below, cells were resuspended in "assay media" consisting of phenol red-free DMEM (Thermo Fisher Scientific, cat. # 21063029) supplemented with 5% charcoal/dextran-treated FBS (Cytiva, cat. # SH30068.03) and 1X pen/strep.

SNU-C4$^{3xFLAG\text{-}LXRβ}$ cells containing a 3xFLAG tag fused to the N-terminus of endogenous LXRβ were generated using CRISPR/Cas9 technology in the Center for Advanced Genome Engineering (St. Jude Children's Research Hospital). Briefly, 1×10^6 SNU-C4 cells were co-transfected with precomplexed ribonuclear proteins (RNPs) consisting of 100 pmol of chemically modified sgRNA (Synthego), 33 pmol of 3xNLS *Sp*Cas9 protein (St. Jude Protein Production Facility), 200 ng of pMaxGFP (Lonza), and 150 pmol of ssODN donor. The transfections were performed via nucleofection (Lonza, 4D-Nucleofector X-unit) using solution SF and program DS-150 in a 20 µL cuvette according to the manufacturer's recommended protocol. GFP+ cells were single-cell sorted five days post-nucleofection (St. Jude Flow Cytometry and Cell Sorting Facility) into 96-well plates containing prewarmed media and were clonally expanded. Clones were screened and verified for the desired modification using targeted deep sequencing, analyzed with CRIS.py as previously described[43,44]. Final clones tested negative for mycoplasma and were authenticated by STR profiling. Editing construct sequences and relevant primers are listed in Supplementary Data 9.

293T$^{CRBN\ KO}$ cells were generated using CRISPR technology in the Center for Advanced Genome Engineering at St. Jude as previously described[45] with the exception that 5×10^5 293T cells were transfected with precomplexed RNPs consisting of 150 pmol of chemically modified sgRNA (SM148.CRBN.g3), 50 pmol of 3X NLS *Sp*Cas9 protein, and 200 ng of pMaxGFP plasmid using solution P3 and program CM-130 in a 20 µL cuvette. Knockout was confirmed by targeted deep sequencing and western blotting (Supplementary Fig. 4).

Compounds

DMSO was purchased from Fisher Scientific (cat. # BP231–100). The PROTACs for our screening library, MD-222 (cat. # HY-134823), MG-277 (cat. # HY-130122), lenalidomide (cat. # HY-A0003), lenalidomide-propargyl-C_2-NH_2 hydrochloride (cat. # HY-130683), MI-1061 (cat. # HY-125858), T0901317 (cat. # HY-10626), SR12813 (cat. # HY-100793), GW3965 (cat. # HY-10627A), and SR9238 (cat. # HY-101442) were purchased from MedChemExpress. Rifampicin (cat. # R3501-5G) and MG-132 (cat. # 474790-10MG) were purchased from MilliporeSigma. 5-

FAM-PMDM6 (cat. # AS-63359-1) was purchased from AnaSpec. SPA70 and SJB7 were synthesized by WuXi AppTec[28]. SJYHJ-040, SJYHJ-073, and SJPYT-214 were synthesized as previously described[27]. SJPYT-328 and SJPYT-331 were synthesized as previously described[34]. BODIPY FL thalidomide was synthesized as previously described[46]. SJYHJ-123, SJYHJ-048, SJYHJ-059, and SJYHJ-108 were synthesized according to procedures presented in the Supplemental Information. The chemical structures and activities of all relevant compounds are shown in Supplementary Data 1.

Plasmids, antibodies, and recombinant proteins

Construction of pcDNA3-HiBiT-PXR containing HiBiT-tagged PXR[18], pcDNA3-HA-CRBN containing HA-tagged CRBN[19], pcDNA3-LgBiT-CRBN containing LgBiT-tagged CRBN[18], pcDNA3-SmBiT-PXR LBD containing SmBiT-tagged PXR LBD (residues 139-434)[47], pGL3-CYP3A4-luc containing firefly luciferase under the control of a PXR-responsive *CYP3A4* promoter[48], pBIND-SRC-1 containing SRC-1 (residues 621-765) fused to GAL4 DBD[49], pcDNA3-FLAG-PXR containing FLAG-tagged PXR[48], pcDNA3-FLAG-PXR 3xW[31], pcDNA3-FLAG-PXR L428Y[34], pcDNA3-HA-VHL containing HA-tagged VHL[18], and pETDuet-1-PXR LBD-mSRC-1 for bacterial expression of His-tagged PXR LBD (residues 130-434) and untagged mouse SRC-1 (residues 623-710)[28] has been described. His6-TEV-CRBN-midi for bacterial expression of truncated and stabilized CRBN was a gift from Alessio Ciulli (Addgene plasmid # 215330)[50]. The sequences and cloning procedures for additional plasmids used in this study are shown in Supplementary Data 10.

Mouse anti-FLAG M2 antibody was purchased from MilliporeSigma (cat. # F3165-5MG). Rabbit anti-β-actin antibody was purchased from Cell Signaling Technology (cat. # 4967L). Rabbit anti-MDM2 (cat. # ab259265) and rabbit anti-GSPT1 (cat. # ab126090) were purchased from Abcam. Rabbit anti-CRBN (cat. # HPA045910-100UL) was purchased from MilliporeSigma. IRDye 800CW goat anti-mouse (cat. # 926-32210) and IRDye 680LT goat anti-rabbit (cat. # 926-68021) were purchased from LI-COR Biotech. LanthaScreen Tb-anti-GST antibody (cat. # PV3550), LanthaScreen Elite Tb-anti-His (cat. # PV5895), and Alexa Fluor 488-anti-GST (cat. # MA4–004-A488) were purchased from Thermo Fisher Scientific.

His-tagged PXR LBD was expressed and purified as previously described[18,51,52]. GST-PXR LBD protein was purchased from Thermo Fisher Scientific (cat. # PV4841). His-tagged CRBN/DDB1 complex was purified as previously described[46,53]. GST-tagged CRBN/DDB1 complex and GST-tagged MDM2 were cloned, expressed, and purified by GenScript. Two proteins (His-PXR LBD-AviLoop and $CRBN^{midi}$) were expressed and purified solely for SPR, and these protocols are below.

pETDuet-His-PXR LBD-AviLoop-mSRC-1 was used to co-express His-tagged PXR LBD (residues 130-434) with an AviTag between positions 184 and 185 and untagged mouse SRC-1 (residues 623–710). pRSF-MBP-TEV-BirA was used to additionally co-express MBP-fused BirA for in vivo biotinylation of the AviTag, similar to a previously reported protocol[54]. The two plasmids (10 ng each) were transformed into BL21(DE3) Competent *E. coli* (New England Biolabs, cat. # C2527H) and grown at 37 °C in terrific broth + 0.2% glucose + 50 μg/mL ampicillin + 25 μg/mL kanamycin to an OD_{600} of 3-4. IPTG (500 μM), and biotin (200 μM) were added, and cells were shaken overnight at 16 °C. Cells were pelleted by centrifugation at 4,000 × *g*, resuspended in lysis buffer [20 mM Tris (pH 7.5), 250 mM NaCl, 5% glycerol, 10 mM imidazole] supplemented with SIGMAFAST Protease Inhibitor Cocktail Tablets, EDTA-Free (MilliporeSigma, cat. # S8830), lysed by sonication, and centrifuged at 20,000 × *g* for 1 h. The supernatant was applied to a 5 mL HisTrap FF column (Cytiva, cat. # 17525501), the column was washed with 50 mL lysis buffer, 25 mL lysis buffer + 50 mM imidazole, and 25 mL lysis buffer + 100 mM imidazole, and PXR LBD was eluted in lysis buffer + 500 mM imidazole. Unlabeled SRC-1 peptide (N-CPSSHSSLTERHKILHRLLQEGSPS-C, prepared by the Hartwell Center Macromolecular Synthesis Section at St. Jude Children's Research Hospital) was added to the eluted protein in a 2:1 molar ratio, and the protein was concentrated to 1.4 mg/mL while buffer exchanging to 20 mM Tris (pH 7.8), 200 mM NaCl, 5% (v/v) glycerol, 5 mM DTT, 2.5 mM EDTA in an Amicon Ultra-15 centrifugal filter unit with 10 kDa cutoff (MilliporeSigma, cat. # UFC901024). Protein was flash frozen in liquid nitrogen and stored at −80 °C.

$CRBN^{midi}$ was expressed and purified as previously described, with modifications[50]. His6-TEV-CRBN-midi plasmid was transformed into BL21(DE3) Competent *E. coli*, grown in LB + 50 μg/mL kanamycin at 37 °C to an OD_{600} of 0.6, and induced overnight at 18 °C with 500 μM IPTG. Cells were pelleted by centrifugation at 4000 × *g*, resuspended in lysis buffer [20 mM HEPES (pH 8.0), 500 mM NaCl, 0.5 mM TCEP, 50 μM $ZnCl_2$, 0.05% Tween-20, 5 mM imidazole, 1 mM $MgCl_2$], lysed by two passages through a microfluidizer at 18,000 psi, and centrifuged at 30,000 × *g* for 2 h. The supernatant was applied to a 5 mL HisTrap FF column, the column was washed with 10 mL of 76% Buffer A [20 mM HEPES (pH 8.0), 500 mM NaCl, 0.5 mM TCEP] and 24% Buffer B [20 mM HEPES (pH 8.0), 500 mM NaCl, 0.5 mM TCEP, 250 mM imidazole], and protein was eluted with a 75 mL linear gradient of 24% Buffer B to 100% Buffer B. Elution fractions were collected and analyzed by SDS–PAGE for protein amount and purity. Selected fractions were pooled, exchanged to Buffer A using a 53 mL HiPrep 26/10 desalting column with Sephadex G-25 resin (Cytiva, cat. # 17508701), and incubated at 4 °C overnight with His-tagged TEV protease to remove the His tag from $CRBN^{midi}$ (2 mg TEV protease for 20 mg $CRBN^{midi}$). The mixture was passed through a 5 mL HisTrap FF column, the flowthrough was collected, and the column was gently washed with Buffer A + 20 mM imidazole to collect loosely bound untagged $CRBN^{midi}$. The cleaved protein was exchanged to storage buffer [20 mM HEPES (pH 7.5), 500 mM NaCl, 0.5 mM TCEP] using a 53 mL HiPrep 26/10 desalting column with Sephadex G-25 resin, concentrated to 3.7 mg/mL in an Amicon Ultra-15 centrifugal filter unit with 10 kDa cutoff, flash frozen in liquid nitrogen, and stored at −80 °C.

$SNU\text{-}C4^{HiBiT\text{-}PXR}$ degradation assays

$SNU\text{-}C4^{HiBiT\text{-}PXR}$ cells suspended in assay media were plated in white tissue culture-treated 384-well plates (Revvity, cat. # 6007680, 1×10^4 cells/well in 25 μL media). The following day, an Echo 655T Acoustic Liquid Handler (Beckman Coulter) was used to dispense 25-125 nL/well of DMSO or stock compounds, depending on the experiment. For experiments with competing ligands, 25 nL of 10 mM competitor was also dispensed for a final concentration of 10 μM. The resulting DMSO concentration was 0.1-0.6%, but a single DMSO concentration was used in each individual experiment. The plates were incubated at 37 °C for the indicated time points, and the Nano-Glo HiBiT Lytic Detection System (Promega, cat. # N3050) and an EnVision microplate reader (Revvity) were used to measure HiBiT signal. DMSO-treated $SNU\text{-}C4^{HiBiT\text{-}PXR}$ cells served as positive controls, and DMSO-treated parental SNU-C4 cells served as negative controls. The percent HiBiT signal for each well was calculated using Eq. 1,

$$\%\ HiBiT\ Signal = 100\% \times \frac{\left(Signal_{HiBiT\ Compound} - Signal_{SNU-C4\ DMSO}\right)}{\left(Signal_{HiBiT\ DMSO} - Signal_{SNU-C4\ DMSO}\right)} \quad (1)$$

For experiments with siRNAs, $SNU\text{-}C4^{HiBiT\text{-}PXR}$ cells (7.5×10^5/well in 1.2 mL culture media) were reverse-transfected in tissue culture-treated six-well plates (Corning, cat. # 353046) with 25 nM siRNA using Lipofectamine RNAiMAX Transfection Reagent (Thermo Fisher Scientific, cat. # 13778150). The following day, the media was replaced with fresh culture media. After an additional 24 h, cells were trypsinized, resuspended in assay media, and plated in white tissue culture-treated 384-well plates (1×10^4 cells/well in 25 μL media). After another 24 h, an Echo 655T Acoustic Liquid Handler was used to dispense 75

nL/well of DMSO or MD-224 stock solutions, resulting in 0.3% DMSO and the indicated MD-224 concentrations. Cells were incubated at 37 °C for 2 h and assayed as above. The signal was normalized to the DMSO controls for the corresponding siRNA transfections. Non-targeting siGENOME siRNA (cat. # D-001210-05-05) and siRNAs targeting *CRBN* (cat. # M-021086-01-0005), *MDM2* (cat. # M-003279-04-0005), *DDB1* (cat. # M-012890-02-0005), *RBX1* (cat. # M-004087-01-0005), *CUL4A* (cat. # M-012610-01-0005), *CUL4B* (cat. # M-017965-01-0005), *UBA52* (cat. # M-011794-01-0005), *RPS27A* (cat. # M-013722-00-0005), *UBB* (cat. # M-013382-01-0005), and *UBC* (cat. # M-019408-01-0005) were purchased from Horizon Discovery.

Western blot analysis

SNU-C4$^{3xFLAG\text{-}PXR}$ or SNU-C4$^{3xFLAG\text{-}LXR\beta}$ cells suspended in assay media were plated in tissue culture-treated 12-well plates (Corning, cat. # 3512, 1 × 10^6 cells/well in 1 mL media). The following day, DMSO or compounds were added to result in 0.5% DMSO and the indicated compound concentrations, and cells were incubated at 37 °C for the indicated time points. Cells were washed with DPBS, trypsinized, pelleted by centrifugation, and lysed in 40 μL radioimmunoprecipitation assay (RIPA) buffer [50 mM Tris (pH 8.0), 150 mM NaCl, 1% NP-40, 0.5% sodium deoxycholate, 0.1% SDS] supplemented with Halt Protease Inhibitor Cocktail (Thermo Fisher Scientific, cat. # 78438). Protein in the lysate was quantified with the Pierce BCA Protein Assay Kit (Thermo Fisher Scientific, cat. # 23227), and 25 μg was diluted with NuPAGE LDS Sample Buffer (cat. # NP0007) and NuPAGE Sample Reducing Agent (cat. # NP0009, Thermo Fisher Scientific), heated at 95 °C for 5 min, and loaded into NuPAGE 4-12% Bis-Tris gels (Thermo Fisher Scientific). Separated proteins were transferred to nitrocellulose membranes using the iBlot 2 Dry Blotting System (Thermo Fisher Scientific). Membranes were blocked with TBST [50 mM Tris (pH 7.4), 150 mM NaCl, 0.1% Tween 20] containing 5% milk for 1 h at room temperature. Antibodies against FLAG (1:2,000 dilution), GSPT1 (1:4,000 dilution), β-actin (1:2,000 dilution), MDM2 (1:1,000 dilution), or CRBN (1:2,000 dilution) were bound overnight at 4 °C in TBST containing 5% milk. Membranes were washed with TBST three times for 10 min each, and LI-COR IRDye secondary antibodies (1:10,000 dilution) were added in TBST containing 5% milk for 1 h at room temperature. Membranes were washed as above and imaged with an Odyssey CLx imaging system (LI-COR). Bands were quantified with Image Studio Lite Software (LI-COR). Selected blots were stripped with NewBlot Nitro Stripping Buffer for Nitrocellulose Membranes (LI-COR, cat. # 928-40030) and reprobed as needed.

For experiments with siRNAs, SNU-C4$^{3xFLAG\text{-}PXR}$ cells (3 × 10^5/well in 600 μL culture media) suspended in culture media were reverse-transfected in tissue culture-treated 12-well plates with 25 nM siRNA using Lipofectamine RNAiMAX. The following day, the media was replaced with fresh culture media. After an additional 48 h, cells were washed with DPBS, and assay media containing 0.5% DMSO +/− 1 μM MD-224 was added. Cells were incubated at 37 °C for 2 h and assayed as above. The signal was normalized to DMSO-treated siNT cells. The same siRNA products were used for the SNU-C4$^{HiBiT\text{-}PXR}$ experiments, with the addition of siGENOME siRNA targeting *PXR* (cat. # M-003415-02-0005) from Horizon Discovery.

PHH plated in six-well plates were obtained through the Human Hepatocyte Isolation Distribution (University of Pittsburgh) and cultured in Williams' Medium E supplemented with Primary Hepatocyte Maintenance Supplement (2 mL media/well). DMSO or compounds were added to result in 0.5% DMSO and the indicated compound concentrations. After 24 h, cells were harvested and analyzed as above using 50 μL RIPA buffer. For donors 1-2, three biological replicates were analyzed. For donor 3, two biological replicates were analyzed.

For blotting HiBiT-tagged PXR in 293T, cells (6 × 10^5/well in 2 mL culture media) were plated in tissue culture-treated six-well plates. The following day, cells were co-transfected with pcDNA3-HiBiT plasmid containing protein of interest (20 ng/well) and pcDNA3-HA-CRBN (20 ng/well) using Lipofectamine 3000 Transfection Reagent (Thermo Fisher Scientific, cat. # L3000015). Empty vector (pcDNA3, 960 ng/well) was used as carrier DNA to increase the total transfected DNA to 1 μg/well. Twenty-four hours after transfection, cells were trypsinized and suspended in assay media, and 5 × 10^5 cells/well in 1 mL media were added to tissue culture-treated 12-well plates. After an additional 24 h, DMSO or compounds were added to result in 0.5% DMSO and the indicated compound concentrations, and cells were incubated at 37 °C for 2 h before lysis and gel loading as above. Membranes were probed for HiBiT-PXR with the Nano-Glo HiBiT Blotting System (Promega, cat. # N2410) and imaged with an Azure 300 imager (Azure Biosystems). Membranes were then blotted for β-actin, imaged with an Odyssey CLx imaging system, and quantified as above.

For blotting FLAG-PXR in 293T, cells (5 × 10^5/well in 800 μL culture media in tissue culture-treated 12-well plates) were reverse-transfected with pcDNA3-FLAG plasmid containing WT or mutant PXR (100 ng/well), pcDNA3-HA-CRBN (100 ng/well), pcDNA3-HA-VHL (100 ng/well), and empty vector (pcDNA3, 1.2 μg/well) using 4.5 μL/well FuGENE 6 Transfection Reagent (Promega, cat. # E2691). Reverse transfections were performed as a bulk batch for each FLAG-PXR construct and aliquoted into wells to ensure equal protein expression for all treatment conditions. The following day, cells were washed with DPBS, and assay media containing 0.5% DMSO, 1 μM MD-224, or 1 μM SJYHJ-040 was added. Cells were incubated at 37 °C for 24 h and lysed and analyzed as above using antibodies against FLAG and β-actin. All uncropped western blot images are shown in the Source Data file.

Live-cell kinetic HiBiT-PXR degradation

293T cells (6 × 10^5/well in 2 mL culture media) were plated in tissue culture-treated six-well plates. The following day, cells were co-transfected with pcDNA3-HiBiT-PXR (20 ng/well), pcDNA3-LgBiT (20 ng/well), and pcDNA3-HA-CRBN (20 ng/well) using Lipofectamine 3000. Empty vector (pcDNA3, 940 ng/well) was used as carrier DNA to increase the total transfected DNA to 1 μg/well. Twenty-four hours after transfection, cells were trypsinized and suspended in assay media, and 5 × 10^3 cells/well in 20 μL assay media were added to white tissue culture-treated 384-well plates. After 24 h, 5 μL assay media containing 5X Vivazine substrate (Promega, cat. # N2580) was added, plates were incubated at 37 °C for 1 h to equilibrate the signal, an Echo 655T Acoustic Liquid Handler was used to dispense 25 nL DMSO or MD-224 stock solutions into the wells, and luminescence was measured every 2.5 min for 2 h on a CLARIOstar Plus microplate reader (BMG Labtech) at 37 °C. Fold change was calculated by dividing the signal by the DMSO signal at each time point.

RT-qPCR

SNU-C4$^{3xFLAG\text{-}PXR}$ cells suspended in assay media were plated in tissue culture-treated 12-well plates (1 × 10^6/well in 1 mL media). The following day, DMSO or compounds were added to result in 0.5% DMSO and the indicated compound concentrations. After 24 h, cells were washed with DPBS, total RNA was isolated with Maxwell 16 LEV SimplyRNA Tissue Kits (Promega, cat. # AS1280), and cDNA was generated from 1 μg of RNA with the SuperScript VILO cDNA Synthesis Kit (Thermo Fisher Scientific, cat. # 11754050). RT-qPCR was conducted with 2 μL of cDNA using TaqMan Fast Advanced Master Mix (Thermo Fisher Scientific, cat. # 4444557) in an Applied Biosystems 7500 Fast Real-Time PCR System. TaqMan gene expression assays specific for *CYP3A4* (assay ID Hs00604506_m1), *PXR* (assay ID Hs01114267_m1), *GAPDH* (Hs03929097_g1), and *RNA18S* (assay ID Hs03928990_g1) were purchased from Thermo Fisher Scientific. Fold induction values were calculated according to the $2^{-\Delta\Delta Ct}$ method, where ΔCt represents the differences in cycle threshold numbers between the target gene and reference gene, and ΔΔCt represents the relative change in these

differences between the control and treatment groups[55]. *RNA18S* was used as the reference gene for relative quantification of other genes.

PHH plated in six-well plates were obtained through the Human Hepatocyte Isolation Distribution (University of Pittsburgh) and cultured in Williams' Medium E supplemented with Primary Hepatocyte Maintenance Supplement (2 mL media/well). DMSO or compounds were added to result in 0.5% DMSO and the indicated compound concentrations. After 24 h, cells were harvested and analyzed as above. For each donor, three biological replicates were analyzed.

293T HiBiT-tagged protein degradation assays

293T cells (6×10^5/well in 2 mL culture media) were plated in tissue culture-treated six-well plates. The following day, cells were co-transfected with pcDNA3-HiBiT plasmid containing protein of interest (20 ng/well) and pcDNA3-HA-CRBN (20 ng/well) using Lipofectamine 3000. Empty vector (pcDNA3, 960 ng/well) was used as carrier DNA to increase the total transfected DNA to 1 μg/well. Twenty-four hours after transfection, cells were trypsinized and suspended in assay media, and 5×10^3 cells/well in 25 μL media were added to white tissue culture-treated 384-well plates. The following day, an Echo 655T Acoustic Liquid Handler was used to dispense 25-125 nL/well of DMSO or stock compounds, depending on the experiment. For experiments with competing ligands, 25 nL of 10 mM competitor was also dispensed for a final concentration of 10 μM. The resulting DMSO concentration was 0.1%-0.6%, but a single DMSO concentration was used in each individual experiment. The plates were incubated at 37 °C for the indicated time points, and the Nano-Glo HiBiT Lytic Detection System and an EnVision microplate reader were used to measure HiBiT signal. DMSO-treated 293T cells transfected with each HiBiT construct served as positive controls, and DMSO-treated 293T cells transfected only with empty vector (pcDNA3) served as negative controls. The percent HiBiT signal for each well was calculated using Eq. 2,

$$\%\ HiBiT\ Signal = 100\% \times \frac{\left(Signal_{HiBiT\ Compound} - Signal_{pcDNA3\ DMSO}\right)}{\left(Signal_{HiBiT\ DMSO} - Signal_{pcDNA3\ DMSO}\right)} \quad (2)$$

Experiments for SRC-1 competition contained 20 ng pcDNA3-HiBiT-PXR, 20 ng pcDNA3-HA-CRBN, up to 2 μg pBIND-SRC-1, and empty vector (pcDNA3) to bring the total transfected DNA to 2.04 μg/well.

PXR degradation and activity in 293T$^{CRBN\ KO}$ cells

293T$^{CRBN\ KO}$ cells (7×10^5/well in 2 mL culture media) were plated in tissue culture-treated six-well plates. The following day, cells were co-transfected with pcDNA3-HiBiT-PXR (20 ng/well), pGL3-CYP3A4-luc (1 μg/well), and either empty vector (pcDNA3, 40 ng/well) or pcDNA3-HA-CRBN (40 ng/well) using Lipofectamine 3000. Twenty-four hours after transfection, cells were trypsinized and suspended in assay media, and 5×10^3 cells/well in 25 μL media were added to white tissue culture-treated 384-well plates. For degradation assays, an Echo 655T Acoustic Liquid Handler was used to dispense 75 nL/well of DMSO or MD-224 stock solutions, plates were incubated at 37 °C for 2 h, and HiBiT signal was measured and normalized as above. To measure PXR activity, an Echo 655T Acoustic Liquid Handler was used to dispense 75 nL/well of DMSO or MD-224 stock solutions and 25 nL/well of 5 mM rifampicin, resulting in 0.4% DMSO and 5 μM rifampicin in all wells. After 24 h, the SteadyLite Plus Reporter Gene Assay System (Revity, cat. # 6066751) and EnVision microplate reader were used to measure firefly luciferase activity. The values were normalized as fold change relative to the rifampicin-only controls for EV- or CRBN-transfected wells.

NanoBiT CRBN-PXR LBD interaction assays

Nano Luciferase Binary Technology (NanoBiT)[56] was used to assess the interaction of CRBN with PXR LBD. HepG2 cells (7.5×10^5/well in 2 mL culture media) were plated in tissue culture-treated six-well plates. The following day, cells were co-transfected with pcDNA3-SmBiT-PXR LBD (300 ng/well) and pcDNA3-LgBiT-CRBN (300 ng/well) using Lipofectamine 3000. Empty vector (pcDNA3, 400 ng/well) was used as carrier DNA to increase the total transfected DNA to 1 μg/well. Twenty-four hours after transfection, cells were trypsinized and suspended in assay media, and 1×10^4 cells/well in 20 μL media were added to white tissue culture-treated 384-well plates. After 24 h, the Nano-Glo Live Cell Assay System (Promega) was used to assess CRBN interaction with PXR LBD. Plates were equilibrated to room temperature for 15 min, and 5 μL Nano-Glo LCS Dilution Buffer containing 5X Nano-Glo Live Cell Substrate was added. The plates were incubated at room temperature for 15 min to equilibrate the signal, an Echo 655T Acoustic Liquid Handler was used to dispense 125 nL/well of DMSO or stock compounds into the wells, and luminescence was measured every 5 min with a CLARIOstar Plus microplate reader at room temperature. Fold change was calculated by dividing the signal by the DMSO signal at each time point, and the 30 min incubation is presented.

TR-FRET CRBN-PXR LBD interaction assays

7.5 μL/well of 24 nM GST-CRBN/DDB1 (2x) and 12 nM AF488-anti-GST (2x) in TR-FRET buffer 1 [50 mM Tris (pH 7.5), 0.002% Pluronic F-127, 0.01% bovine serum albumin (BSA), and 0.05 mM dithiothreitol (DTT)] was added into black 384-well low-volume assay plates (Revvity, cat. # 6008260). An Echo 655T Acoustic Liquid Handler was then used to dispense 45 nL/well of DMSO or stock compounds. 7.5 μL/well of 6 nM His-PXR LBD (2x) and 6 nM Tb-anti-His (2x) in TR-FRET buffer 1 was then dispensed into the wells. The additions resulted in 15 μL/well of TR-FRET buffer 1 containing 3 nM His-PXR LBD, 3 nM Tb-anti-His, 12 nM GST-CRBN/DDB1, 6 nM AF488-anti-GST, 0.3% DMSO, and the indicated compound concentrations. The plates were shaken at 900 rpm (80 × *g*) on an IKA MTS 2/4 digital microtiter shaker for 1 min, centrifuged at 1,000 rpm (201 × *g*) for 30 s in an Eppendorf 5810 centrifuge equipped with an A-4-62 swinging-bucket rotor, and protected from light exposure and incubated for 90 min at room temperature. The TR-FRET signal from each well was collected with a PHERAstar FS microplate reader (BMG Labtech) using 340 nm excitation, 520 and 490 nm emissions, a 100 μs delay, and a 200 μs integration time. The measured relative fluorescence units (RFU) were normalized for each well using Eq. 3,

$$Signal = \frac{RFU\ at\ 520\ nm}{RFU\ at\ 490\ nm} \times 10^4 \quad (3)$$

Fold change was then calculated by normalizing to DMSO control wells.

TR-FRET PXR LBD competitive binding assays

The PXR LBD competitive binding assays were performed as previously described[27]. 7.5 μL/well of 60 nM fluorescent probe (SJPYT-214 or SJYHJ-073) (2x) in TR-FRET buffer 1 was dispensed into the wells of black 384-well low-volume assay plates. An Echo 655T Acoustic Liquid Handler was then used to dispense 45 nL/well of DMSO or stock compounds. 7.5 μL/well of 6 nM GST-PXR LBD (2x) and 6 nM Tb-anti-GST (2x) was then dispensed into the wells. The additions resulted in 15 μL/well of TR-FRET buffer 1 containing 3 nM GST-PXR LBD, 3 nM Tb-anti-GST, 30 nM fluorescent probe (SJPYT-214 or SJYHJ-073), 0.4% DMSO (0.1% from probe addition and 0.3% from compound addition), and the indicated compound concentrations. The plates were shaken, centrifuged, incubated, measured, and normalized as above.

TR-FRET CRBN competitive binding assays

The CRBN competitive binding assays were performed as previously described[46]. 7.5 μL/well of 8 nM BODIPY FL thalidomide (2x) in TR-FRET buffer 2 [50 mM Tris (pH 7.5), 0.01% Triton X-100, 0.01% BSA, and 1 mM DTT] was dispensed into the wells of black 384-well low-volume assay plates. An Echo 655T Acoustic Liquid Handler was then used to dispense 45 nL/well of DMSO or stock compounds. 7.5 μL/well of 4 nM His-CRBN/DDB1 (2x) and 4 nM Tb-anti-His (2x) in TR-FRET buffer 2 was then dispensed into the wells. The additions resulted in 15 μL/well of TR-FRET buffer 2 containing 2 nM His-CRBN/DDB1, 2 nM Tb-anti-His, 4 nM BODIPY FL thalidomide, 0.4% DMSO (0.1% from BODIPY FL thalidomide addition and 0.3% from compound addition), and the indicated compound concentrations. The plates were shaken, centrifuged, incubated, measured, and normalized as above.

TR-FRET MDM2 competitive binding assays

7.5 μL/well of 6.6 nM 5-FAM-PMDM6 (2x) in TR-FRET buffer 2 was dispensed into the wells of black 384-well low-volume assay plates. An Echo 655T Acoustic Liquid Handler was then used to dispense 45 nL/well of DMSO or stock compounds. 7.5 μL/well of 4 nM GST-MDM2 (2x) and 4 nM Tb-anti-GST (2x) in TR-FRET buffer 2 was then dispensed into the wells. The additions resulted in 15 μL/well of TR-FRET buffer 2 containing 2 nM GST-MDM2, 2 nM Tb-anti-GST, 3.3 nM 5-FAM-PMDM6, 0.4% DMSO (0.1% from 5-FAM-PMDM6 addition and 0.3% from compound addition), and the indicated compound concentrations. The plates were shaken, centrifuged, incubated, measured, and normalized as above.

TR-FRET CRBN-MDM2 interaction assays

7.5 μL/well of 24 nM His-CRBN/DDB1 (2x) and 8 nM AF488-anti-His (2x) in TR-FRET buffer 2 was dispensed into the wells of black 384-well low-volume assay plates. An Echo 655T Acoustic Liquid Handler was then used to dispense 45 nL/well of DMSO or stock compounds. 7.5 μL/well of 6 nM GST-MDM2 (2x) and 6 nM Tb-anti-GST (2x) in TR-FRET buffer 2 was then dispensed into the wells. The additions resulted in 15 μL/well of TR-FRET buffer 2 containing 3 nM GST-MDM2, 3 nM Tb-anti-GST, 12 nM His-CRBN/DDB1, 4 nM AF488-anti-His, 0.3% DMSO, and the indicated compound concentrations. The plates were shaken, centrifuged, incubated, measured, and normalized as above.

Structural analysis

PyMOL (Schrödinger) was used to load and align structures. The crystal structure of PXR LBD bound to the agonist SJPYT-328 (PDB 8SVS) was used as the PXR LBD reference structure. α2 was defined as residues 192-210 for fully modeled structures, and α12 was defined as residues 422–434 for fully modeled structures. For PXR LBD alignments ($n = 65$, Supplementary Data 2), chain A was used for all structures except PDBs 6HTY and 8SVR; in 6HTY, ligand was only modeled in chain B, and in 8SVR, the full ligand was only modeled in chain B. The corresponding SRC-1 peptide chains were retained for all structures. For NR alignments, the crystal structures of PXR LBD (PDB 8SVS, chain A), CAR LBD (PDB 1XVP, chain D), VDR LBD (PDB 1S0Z, chain A), FXR LBD (PDB 3FXV, chain A), LXRα LBD (PDB 3IPQ, chain A), LXRβ LBD (PDB 1P8D, chain A), AR (PDB 2AM9, chain A), and ERα (PDB 1GWR, 1A52, or 2OUZ, all chain A). were used. Chain D was used for CAR LBD because it contained the modeled ligand (CITCO). The corresponding coactivator peptide chains for structures containing the peptide (PDBs 8SVS, 1XVP, 3FXV, 3IPQ, 1P8D, and 1GWR) were retained. For MDM2 bound to SAR405838, chain A of PDB 5TRF was used.

SPR PXR LBD binding assay

SPR experiments were performed on a BIACORE 8 K instrument at 25 °C in 1×HBS-P+ buffer (Cytiva) with 2% DMSO. N-terminal biotin-labeled PXR LBD protein was immobilized on streptavidin-coated SA chip (Flow cell 2) with immobilization level ~8500 RU, and then the multicycle kinetics method with A-B-A injection mode was used. For each injection, a solution (solution A) with either 50 μM T0901317, 10 μM $CRBN^{midi}$, or 50 μM T0901317 mixed with 10 μM $CRBN^{midi}$ in 1× SPR running buffer was injected over the surface at 30 μL/min for 45 s to achieve equilibrium binding (A). Then, MD-224 was serially diluted 1:2 for 6 total concentrations (ranging from 1.56–50 μM) in the presence of each corresponding solution A, and injected over the surface at 30 μL/min for 60 s (B) to measure the binding kinetics, followed by another injection of corresponding solution A over the surface at 30 μL/min for 30 s (A) to allow the dissociation to be monitored. SPR data were double-referenced and analyzed with Biacore Insight Evaluation Software (Cytiva) and fit to steady-state affinity models to determine K_D and R_{max}.

Proteome Profiling by TMT-MS

293T cells were plated in tissue culture-treated 10 cm dishes (3.5×10^6 cells/dish in 10 mL culture media). The following day, cells were co-transfected with pcDNA3-FLAG-PXR (120 ng/dish) and pcDNA3-HA-CRBN (120 ng/dish) using Lipofectamine 3000. Empty vector (pcDNA3, 5.76 μg/dish) was used as carrier DNA to increase the total transfected DNA to 6 μg/dish. These conditions were chosen to match those of the HiBiT degradation assays. Twenty-four hours after transfection, cells were washed with DPBS, and assay media was added to the dishes. After an additional 24 h, 0.5% DMSO, 100 nM MD-224, or 1 μM MD-224 was added to duplicate dishes. After 2 h, the media was removed, and cells were washed twice with ice-cold DPBS, scraped in 10 mL cold DPBS, transferred to 15 mL tubes, and centrifuged at 300 × *g* for 5 min. DPBS was removed, pellets were resuspended in 1 mL cold DPBS and transferred to 1.5 mL tubes, tubes were centrifuged again, DPBS was removed, and dry cell pellets were frozen on dry ice and stored at -80 °C.

TMT-MS sample processing was performed according to a previously optimized protocol[57]. Briefly, the cells were lysed in 50 mM *N*-(2-hydroxyethyl)piperazine-*N*′-ethanesulfonic acid (HEPES) (pH 8.5) containing 8 M urea and 0.5% sodium deoxycholate, and approximately 100 μg of protein per sample was proteolyzed with Lys-C (Wako) [enzyme-to-substrate ratio of 1:100 (w/w)] for 3 h at room temperature followed by dilution with 50 mM HEPES (pH 8.5) to a final 2 M urea concentration. Proteins were further digested with trypsin (Promega) [enzyme-to-substrate ratio of 1:50 (w/w)] overnight at room temperature. Disulfide bonds were reduced with DTT (2 mM and 20 min incubation at room temperature), alkylated with iodoacetamide (10 mM and 30 min incubation at room temperature in the dark), and quenched with DTT (30 mM and 20 min incubation at room temperature). Digestion was stopped by adding formic acid (FA) to 0.5%, and samples were centrifuged at 21,000 × *g* at 4 °C to remove insoluble material, desalted on tC18 SepPak solid-phase extraction cartridges (Waters Corporation), dried by SpeedVac, and stored at -80 °C.

Dried peptides were resuspended in 50 μL of 100 mM HEPES (pH 8.5) and labeled with TMTpro 18plex Label Reagents [Thermo Fisher Scientific, 10 μg/μL in 100% acetonitrile (ACN), 1:2 (w/w) ratio, room temperature for 1 h]. Reactions were quenched by the addition of hydroxylamine to 0.3% (v/v), and labeled peptides were combined equally, acidified with FA [final 0.5% (v/v)], desalted on tC18 SepPak solid-phase extraction cartridges, and dried by SpeedVac. Peptides were reconstituted in Buffer A [10 mM ammonium formate (pH 8)] and fractionated by high pH reversed-phase LC performed on a Xbridge 4.6 mm × 250 mm column (Waters Corporation) with an Agilent 1200 HPLC system using a 180 min gradient of 15%-50% Buffer B [90% ACN, 10 mM ammonium formate (pH 8)] collected into 96 concatenated fractions. Fractions were dried in SpeedVac and resuspended in 5 μL of 5% FA/1% trifluoroacetic acid (TFA) and analyzed by LC-MS/MS on a QE-HF mass spectrometer (Thermo Fisher Scientific) connected in-line to a Dionex Ultimate 3000 ultra-high pressure liquid chromatography system. Peptides were separated on a PepMap 75 μm × 15 cm 1.9 μm

C18 column at 50 °C using a 120 min gradient of 12-56% Buffer B [67% ACN/2.5% DMSO/0.1% FA] at an optimal ~0.250 mL/min flow rate. MS data were collected in the "high-high" data-dependent mode with the MS1 scan in Orbitrap (60,000 resolution, scan range 450-1600 m/z, 1×10^6 AGC target, ~50 ms maximal ion time), followed by data-dependent MS2 scans with cycle of time at 3 seconds in Orbitrap (60,000 resolution, scan range starting from 120 *m/z*, 1×10^5 AGC target, ~105 ms maximal ion time, 34 HCD normalized collision energy, 1.0 m/z isolation window, and 15 s dynamic exclusion, charge state screening enabled to reject precursor charge states that were unassigned, + 1, or > + 4).

MS raw files were converted to mzXML files, and database searches were performed against the Uniprot HUMAN protein database using our in-house developed JUMP pipeline[58]. Search parameters included precursor ions mass tolerance 20 ppm, fragment ions 0.02 Da, fully tryptic with maximal two missed cleavages and maximal three modification sites per peptide, TMT18 modification of Lys residues and of N termini (+ 304.20715 Da), and carbamidomethylation of Cys residues (+ 57.02146 Da) set as static modifications, while Met oxidation (+ 15.99492 Da) was set as dynamic modifications. Peptide-spectrum match filtering was performed based on precursor ion mass accuracy and then grouped by peptide length, tryptic ends, modifications, mis-cleavage sites, and precursor ion charge state as parameters to reduce the false discovery rate below 1% for peptides based on the target-decoy strategy[59]. TMT-based quantification, data quality control, and statistical analysis were performed based on our previous method[60]. Protein fold change and *P* values of different comparisons were calculated based on protein intensities. Differential expression analysis was performed based on our previous method[61].

Proteome profiling by DIA

SNU-C4$^{3xFLAG\text{-}PXR}$ cells suspended in culture media were plated in tissue culture-treated 10 cm dishes (1×10^7/dish in 10 mL media). The following day, cells were washed with DPBS, and assay media was added. After an additional 24 h, the media was removed, and cells were washed twice with ice-cold DPBS, scraped in 10 mL cold DPBS, and transferred to 15 mL tubes. 10% (1 mL) of the suspension was aliquoted for DIA analysis of the total lysate. 30% (3 mL) was aliquoted as a precautionary sample but was not used in any analysis. The remaining 60% (6 mL) was used in subsequent immunoprecipitation (IP). Tubes were centrifuged at 300 × *g* for 5 min. DPBS was removed, and dry cell pellets were frozen on dry ice and stored at -80 °C. For IP, cell pellets were thawed on ice, lysed in 500 μL RIPA buffer supplemented with Halt Protease Inhibitor Cocktail, sonicated at 30% amplitude for 20 s to shear DNA, and centrifuged at 16,000 × *g* for 10 min to remove insoluble material. The supernatant (450 μL) was transferred to new tubes containing 5 μg anti-FLAG antibody and 50 μL Dynabeads Protein G (Thermo Fisher Scientific, cat. # 10004D) that had been washed three times with 1 mL RIPA, and the mixtures were rotated at 4 °C overnight. Beads were collected by placing the tubes on a magnet, the supernatant was removed, beads were washed three times with 500 μL RIPA, and bound proteins were eluted by shaking at 37 °C for 1 h in 50 μL RIPA containing 100 ng/μL 3xFLAG peptide (MilliporeSigma, cat. # F4799).

For 293T analysis, cells (1×10^6/well in 2 mL culture media in tissue culture-treated six-well plates) were reverse transfected with pcDNA3-FLAG-PXR (250 ng/well), pcDNA3-HA-CRBN (250 ng/well), and empty vector (pcDNA3, 1 μg/well) using 4.5 μL/well FuGENE 6 Transfection Reagent. The conditions were chosen to maximize PXR expression while retaining sensitivity to MD-224, and reverse transfections were performed as a bulk batch and aliquoted into wells to ensure equal protein expression for all treatment conditions. The following day, the media was replaced with fresh culture media. After an additional 24 h, the media was removed, cells were washed with DPBS, and 1 mL assay media containing 0.5% DMSO, 100 nM MD-224, or 1 μM MD-224 was added. After 2 h, cells were collected by pipetting the media directly in the wells and transferring to 1.5 mL tubes. Wells were washed with 300 μL DPBS, and the wash was combined with the collected cell sample. Tubes were centrifuged at 300 × *g* for 5 min, the media was removed, 1 mL DPBS was added to wash the cell pellets, tubes were centrifuged again, DPBS was removed, and cell pellets were frozen on dry ice and stored at -80 °C.

Cell pellets were lysed with 50 mM HEPES (pH 8.5) containing 8 M urea. The lysates were digested with Lys-C [enzyme-to-substrate ratio of 1:10 (w/w)] for 30 min at room temperature. Following Lys-C digestion, the samples were diluted to 2 M urea with 50 mM HEPES (pH 8.5) and further digested with trypsin [enzyme-to-substrate ratio of 1:10 (w/w)] for 3 h at room temperature. The digests were acidified with 5% FA, and 25% (approximately 0.5-1 μg) of the digests were loaded on Evotips (Evosep Biosystems) following the manufacturer's recommendations. IP samples were run on short gels as previously described[62]. Proteins in gel bands were reduced with 10 mM DTT and alkylated by 25 mM iodoacetamide. The gel bands were then washed, dried, and rehydrated with a buffer containing trypsin. Samples were digested overnight and acidified, and the peptides were extracted. The extracts were dried and reconstituted in 5% FA. 30% (approximately 0.5-1 μg) of the digests were loaded on Evotips following the manufacturer's recommendations. Samples were analyzed on a Bruker timsTOF HT instrument coupled to EvosepOne (Evosep Biosystems) using a 30 samples per day method. An Evosep column (15 cm × 150 μm, 1.5 μm C18 particles) was used for peptide separation. Data was acquired using the dia-PASEF mode with an MS1 scan range of 100-1700 *m/z*. 21 isocratic *m/z* and ion mobility windows were selected for serial MS2 fragmentation ranging from 475 to 1000 *m/z* and 0.7 to 1.3 1/K0 respectively.

The raw timsTOF data (.d folders) were imported into DIA-NN (version 2.1)[63,64] and analyzed with the library-free mode. Human protein sequences (proteome ID: UP000005640, 81,791 proteins) were downloaded from UniProt database (version 2024/11/27). The protein FASTA file was then used for in silico library generation with the following settings: Trypsin/P with maximum 2 missed cleavage; oxidation on methionine as variable modification; maximum number of variable modifications set to 2; peptide length from 7 to 30; precursor charge 1–4; precursor *m/z* from 400 to 1200; fragment *m/z* from 200 to 1800. The search parameters of DIA-NN were set as follows: precursor FDR 1%; mass accuracy at MS1 and MS2 both set to 20 ppm; scan window set to 0 (automatic inference); isotopologues and MBR (match-between-run) turned on; no shared spectra enabled; protein inference at gene level; heuristic protein inference enabled; quantification strategy set to robust LC (high precision); neural network classifier single-pass mode; cross-run normalization turned off; library generation set to smart profiling; speed and RAM usage set to optimal results. The search results were further filtered with precursor *q* value < 0.01 and protein group *q* value < 0.01 at the library level. For quantification, DIA-NN first obtained precursor quantities by summing the intensities of the top six fragments (ranked by their library intensities) for each precursor. Precursors corresponding to unique proteins were then used for protein-level quantification, and intensities of protein groups were obtained using the MaxLFQ algorithm implemented in the iq r package[65]. Proteins were log2 transformed and normalized using the median followed by statistical analysis using proteoDA, which performs limma moderated t-test with empirical Bayes smoothing applied to the standard errors[66].

Plotting and statistical analyses

All plots were made in GraphPad Prism 10. Results are expressed as the mean ± standard deviation from at least three independent experiments, with the exception of TMT-MS, which was performed in duplicate. Individual points on bar graphs represent biological

replicates. Sigmoidal or bell-shaped dose response curves were fitted as needed. The degradation index was calculated by converting DC_{50} to pDC_{50} (negative log of DC_{50} in molar) and multiplying by D_{max}.

Reporting summary

Further information on research design is available in the Nature Portfolio Reporting Summary linked to this article.

Data availability

All TMT-MS RAW files are available via ProteomeXchange with identifier PXD059473. All DIA-MS RAW files are available via ProteomeXchange with identifier PXD066110. All PXR LBD structures used in analysis (n = 65) are presented in Supplementary Data 2. Additional crystal structures used in this study are 1XVP (CAR LBD), 1S0Z (VDR LBD), 3FXV (FXR LBD), 3IPQ (LXRα LBD), 1P8D (LXRβ LBD), 2AM9 (AR LBD), 1GWR (ERα LBD), 1A52 (ERα LBD), 2OUZ (ERα LBD), and 5TRF (MDM2). Source data are provided with this paper.

References

1. Lambert, S. A. et al. The Human Transcription Factors. *Cell* **172**, 650–665 (2018).
2. Henley, M. J. & Koehler, A. N. Advances in targeting 'undruggable' transcription factors with small molecules. *Nat. Rev. Drug Discov.* https://doi.org/10.1038/s41573-021-00199-0 (2021).
3. Winter, G. E. et al. Phthalimide conjugation as a strategy for in vivo target protein degradation. *Science* **348**, 1376–1381 (2015).
4. Kronke, J. et al. Lenalidomide causes selective degradation of IKZF1 and IKZF3 in multiple myeloma cells. *Science* **343**, 301–305 (2014).
5. Ito, T. et al. Identification of a primary target of thalidomide teratogenicity. *Science* **327**, 1345–1350 (2010).
6. Lu, G. et al. The myeloma drug lenalidomide promotes the cereblon-dependent destruction of Ikaros proteins. *Science* **343**, 305–309 (2014).
7. Chamberlain, P. P. & Hamann, L. G. Development of targeted protein degradation therapeutics. *Nat. Chem. Biol.* **15**, 937–944 (2019).
8. Sakamoto, K. M. et al. Protacs: chimeric molecules that target proteins to the Skp1-Cullin-F box complex for ubiquitination and degradation. *Proc. Natl. Acad. Sci. USA* **98**, 8554–8559 (2001).
9. Evans, R. M. & Mangelsdorf, D. J. Nuclear receptors, RXR, and the big bang. *Cell* **157**, 255–266 (2014).
10. Santos, R. et al. A comprehensive map of molecular drug targets. *Nat. Rev. Drug Discov.* **16**, 19–34 (2017).
11. Webb, P., Lopez, G. N., Uht, R. M. & Kushner, P. J. Tamoxifen activation of the estrogen receptor/AP-1 pathway: potential origin for the cell-specific estrogen-like effects of antiestrogens. *Mol. Endocrinol.* **9**, 443–456 (1995).
12. Dauvois, S., Danielian, P. S., White, R. & Parker, M. G. Antiestrogen ICI 164,384 reduces cellular estrogen receptor content by increasing its turnover. *Proc. Natl. Acad. Sci. USA* **89**, 4037–4041 (1992).
13. Bondeson, D. P. & Crews, C. M. Targeted Protein Degradation by Small Molecules. *Annu. Rev. Pharm. Toxicol.* **57**, 107–123 (2017).
14. Grinshpun, A. Clinician's guide to targeted estrogen receptor degradation using PROTAC in patients with estrogen receptor-positive metastatic breast cancer. *Curr. Opin. Oncol.* **35**, 472–478 (2023).
15. Bondeson, D. P. et al. Catalytic in vivo protein knockdown by small-molecule PROTACs. *Nat. Chem. Biol.* **11**, 611–617 (2015).
16. Salami, J. et al. Androgen receptor degradation by the proteolysis-targeting chimera ARCC-4 outperforms enzalutamide in cellular models of prostate cancer drug resistance. *Commun. Biol.* **1**, 100 (2018).
17. Xu, H. et al. Development of Agonist-Based PROTACs Targeting Liver X Receptor. *Front. Chem.* **9**, 674967 (2021).
18. Huber, A. D., Lin, W., Poudel, S., Miller, D. J. & Chen, T. PROTAC-mediated activation, rather than degradation, of a nuclear receptor reveals complex ligand-receptor interaction network. *Structure* **32**, 2352–2363.e2358 (2024).
19. Huber, A. D. et al. SJPYT-195: A Designed Nuclear Receptor Degrader That Functions as a Molecular Glue Degrader of GSPT1. *ACS Med. Chem. Lett.* **13**, 1311–1320 (2022).
20. Bertilsson, G. et al. Identification of a human nuclear receptor defines a new signaling pathway for CYP3A induction. *Proc. Natl. Acad. Sci. USA* **95**, 12208–12213 (1998).
21. Blumberg, B. et al. SXR, a novel steroid and xenobiotic-sensing nuclear receptor. *Genes Dev.* **12**, 3195–3205 (1998).
22. Kliewer, S. A. et al. An orphan nuclear receptor activated by pregnanes defines a novel steroid signaling pathway. *Cell* **92**, 73–82 (1998).
23. Lehmann, J. M. et al. The human orphan nuclear receptor PXR is activated by compounds that regulate CYP3A4 gene expression and cause drug interactions. *J. Clin. Invest.* **102**, 1016–1023 (1998).
24. Synold, T. W., Dussault, I. & Forman, B. M. The orphan nuclear receptor SXR coordinately regulates drug metabolism and efflux. *Nat. Med.* **7**, 584–590 (2001).
25. Li, Y. et al. Discovery of MD-224 as a First-in-Class, Highly Potent, and Efficacious Proteolysis Targeting Chimera Murine Double Minute 2 Degrader Capable of Achieving Complete and Durable Tumor Regression. *J. Med. Chem.* **62**, 448–466 (2019).
26. Florke Gee, R. R. et al. The F-box-only protein 44 regulates pregnane X receptor protein level by ubiquitination and degradation. *Acta Pharm. Sin. B* **13**, 4523–4534 (2023).
27. Huber, A. D. et al. First-in-Class Small Molecule Degrader of Pregnane X Receptor Enhances Chemotherapy Efficacy. *J. Med. Chem.* **67**, 18549–18575 (2024).
28. Lin, W. et al. SPA70 is a potent antagonist of human pregnane X receptor. *Nat. Commun.* **8**, 741 (2017).
29. Watkins, R. E. et al. The human nuclear xenobiotic receptor PXR: structural determinants of directed promiscuity. *Science* **292**, 2329–2333 (2001).
30. Watkins, R. E., Davis-Searles, P. R., Lambert, M. H. & Redinbo, M. R. Coactivator binding promotes the specific interaction between ligand and the pregnane X receptor. *J. Mol. Biol.* **331**, 815–828 (2003).
31. Huber, A. D. et al. Mutation of a single amino acid of pregnane X receptor switches an antagonist to agonist by altering AF-2 helix positioning. *Cell Mol. Life Sci.* **78**, 317–335 (2021).
32. Petzold, G. et al. Mining the CRBN target space redefines rules for molecular glue-induced neosubstrate recognition. *Science* **389**, eadt6736 (2025).
33. Wang, H. et al. The phytoestrogen coumestrol is a naturally occurring antagonist of the human pregnane X receptor. *Mol. Endocrinol.* **22**, 838–857 (2008).
34. Garcia-Maldonado, E. et al. Chemical manipulation of an activation/inhibition switch in the nuclear receptor PXR. *Nat. Commun.* **15**, 4054 (2024).
35. Yang, J. et al. Simple Structural Modifications Converting a Bona fide MDM2 PROTAC Degrader into a Molecular Glue Molecule: A Cautionary Tale in the Design of PROTAC Degraders. *J. Med. Chem.* **62**, 9471–9487 (2019).
36. Wang, S. et al. SAR405838: an optimized inhibitor of MDM2-p53 interaction that induces complete and durable tumor regression. *Cancer Res.* **74**, 5855–5865 (2014).
37. Bouguenina, H. et al. A Degron Blocking Strategy Towards Improved CRL4(CRBN) Recruiting PROTAC Selectivity. *Chembiochem* **24**, e202300351 (2023).
38. Kumar, N. et al. The benzenesulfoamide T0901317 [N-(2,2,2-trifluoroethyl)-N-[4-[2,2,2-trifluoro-1-hydroxy-1-(trifluoromethyl)ethyl]

phenyl]-benzenesulfonamide] is a novel retinoic acid receptor-related orphan receptor-alpha/gamma inverse agonist. *Mol. Pharm.* **77**, 228–236 (2010).
39. Li, H. et al. Novel yeast-based strategy unveils antagonist binding regions on the nuclear xenobiotic receptor PXR. *J. Biol. Chem.* **288**, 13655–13668 (2013).
40. Shang, J. et al. A molecular switch regulating transcriptional repression and activation of PPARgamma. *Nat. Commun.* **11**, 956 (2020).
41. Bondeson, D. P. et al. Lessons in PROTAC Design from Selective Degradation with a Promiscuous Warhead. *Cell Chem. Biol.* **25**, 78–87.e75 (2018).
42. Nowak, R. P. et al. Plasticity in binding confers selectivity in ligand-induced protein degradation. *Nat. Chem. Biol.* **14**, 706–714 (2018).
43. Connelly, J. P. & Pruett-Miller, S. M. CRIS.py: A Versatile and High-throughput Analysis Program for CRISPR-based Genome Editing. *Sci. Rep.* **9**, 4194 (2019).
44. Narina, S., Connelly, J. P. & Pruett-Miller, S. M. High-Throughput Analysis of CRISPR-Cas9 Editing Outcomes in Cell and Animal Models Using CRIS.py. *Methods Mol. Biol.* **2631**, 155–182 (2023).
45. Nishiguchi, G. et al. Selective CK1alpha degraders exert anti-proliferative activity against a broad range of human cancer cell lines. *Nat. Commun.* **15**, 482 (2024).
46. Lin, W. et al. Development of BODIPY FL Thalidomide As a High-Affinity Fluorescent Probe for Cereblon in a Time-Resolved Fluorescence Resonance Energy Transfer Assay. *Bioconjug. Chem.* **31**, 2564–2575 (2020).
47. Huber, A. D. et al. A bromodomain-independent mechanism of gene regulation by the BET inhibitor JQ1: direct activation of nuclear receptor PXR. *Nucleic Acids Res* **52**, 1661–1676 (2024).
48. Lin, W. et al. Cyclin-dependent kinase 2 negatively regulates human pregnane X receptor-mediated CYP3A4 gene expression in HepG2 liver carcinoma cells. *J. Biol. Chem.* **283**, 30650–30657 (2008).
49. Pondugula, S. R. et al. A phosphomimetic mutation at threonine-57 abolishes transactivation activity and alters nuclear localization pattern of human pregnane x receptor. *Drug Metab. Dispos.* **37**, 719–730 (2009).
50. Kroupova, A. et al. Design of a Cereblon construct for crystallographic and biophysical studies of protein degraders. *Nat. Commun.* **15**, 8885 (2024).
51. Huber, A. D. et al. Ligand flexibility and binding pocket malleability cooperate to allow selective PXR activation by analogs of a promiscuous nuclear receptor ligand. *Structure* **31**, 1545–1555 e1549 (2023).
52. Lin, W. et al. Structure-guided approach to modulate small molecule binding to a promiscuous ligand-activated protein. *Proc. Natl. Acad. Sci. USA* **120**, e2217804120 (2023).
53. Lin, W. & Chen, T. General Stepwise Approach to Optimize a TR-FRET Assay for Characterizing the BRD/PROTAC/CRBN Ternary Complex. *ACS Pharm. Transl. Sci.* **4**, 941–952 (2021).
54. Li, Y. & Sousa, R. Novel system for in vivo biotinylation and its application to crab antimicrobial protein scygonadin. *Biotechnol. Lett.* **34**, 1629–1635 (2012).
55. Livak, K. J. & Schmittgen, T. D. Analysis of relative gene expression data using real-time quantitative PCR and the 2(-Delta Delta C(T)) Method. *Methods* **25**, 402–408 (2001).
56. Dixon, A. S. et al. NanoLuc complementation reporter optimized for accurate measurement of protein interactions in cells. *ACS Chem. Biol.* **11**, 400–408 (2016).
57. High, A. A. et al. Deep Proteome Profiling by Isobaric Labeling, Extensive Liquid Chromatography, Mass Spectrometry, and Software-assisted Quantification. *J Vis Exp* https://doi.org/10.3791/56474 (2017).
58. Wang, X. et al. JUMP: a tag-based database search tool for peptide identification with high sensitivity and accuracy. *Mol. Cell Proteom.* **13**, 3663–3673 (2014).
59. Peng, J., Elias, J. E., Thoreen, C. C., Licklider, L. J. & Gygi, S. P. Evaluation of multidimensional chromatography coupled with tandem mass spectrometry (LC/LC-MS/MS) for large-scale protein analysis: the yeast proteome. *J. Proteome Res.* **2**, 43–50 (2003).
60. Niu, M. et al. Extensive Peptide Fractionation and y(1) Ion-Based Interference Detection Method for Enabling Accurate Quantification by Isobaric Labeling and Mass Spectrometry. *Anal. Chem.* **89**, 2956–2963 (2017).
61. Bai, B. et al. Deep multilayer brain proteomics identifies molecular networks in Alzheimer's disease progression. *Neuron* **105**, 975–991 e977 (2020).
62. Xu, P., Duong, D. M. & Peng, J. Systematical optimization of reverse-phase chromatography for shotgun proteomics. *J. Proteome Res* **8**, 3944–3950 (2009).
63. Demichev, V., Messner, C. B., Vernardis, S. I., Lilley, K. S. & Ralser, M. DIA-NN: neural networks and interference correction enable deep proteome coverage in high throughput. *Nat. Methods* **17**, 41–44 (2020).
64. Demichev, V. et al. dia-PASEF data analysis using FragPipe and DIA-NN for deep proteomics of low sample amounts. *Nat. Commun.* **13**, 3944 (2022).
65. Pham, T. V., Henneman, A. A. & Jimenez, C. R. iq: an R package to estimate relative protein abundances from ion quantification in DIA-MS-based proteomics. *Bioinformatics* **36**, 2611–2613 (2020).
66. Thurman, T. J. et al. proteoDA: a package for quantitative proteomics. *J. Open Source Softw.* **8** https://doi.org/10.21105/joss.05184 (2023).

Acknowledgements

Research reported in this publication was supported by the National Institute of General Medical Sciences of the National Institutes of Health (NIH) under award number R35GM118041 (to T.C.). RF1AG064909 (to J.P.) supported the proteome profiling by TMT-MS. Research was also supported by work conducted in the Center for Advanced Genome Engineering (St. Jude), The Hartwell Center for Biotechnology (St. Jude), and the Center for Proteomics and Metabolomics (St. Jude), which are supported in part by the National Cancer Institute grant P30CA021765. The content is solely the responsibility of the authors and does not necessarily represent the official views of the National Institutes of Health. The authors thank ALSAC for support, Yifan Zhang for TEV protease purification, and members of the Chen laboratory for valuable discussion. This work utilized hepatocytes obtained through the Human Hepatocyte Isolation Distribution (University of Pittsburgh), part of the Pittsburgh Liver Research Center Clinical Biospecimen Repository and Processing Core, Pittsburgh, Pennsylvania, which was funded by grant P30DK120531, now called the Human Liver Tissue and Hepatocyte Research Resource funded by grant R24DK139775.

Author contributions

A.D.H. and T.C. conceived the work. A.D.H., W.L., S.P., G.Y., J. Wu, A.G.C., and R.R.F.G. designed and conducted experiments. Y.-H.J. synthesized compounds. V.P., W.W., Y.F., Z.-F.Y., and S.D.B. conducted and analyzed DIA experiments. K.Y. and J.P. conducted and analyzed TMT-MS experiments. E.D.A., A.J.L., and S.M.P.-M. generated CRISPR/Cas9 cell lines. J. Wang purified $CRBN^{midi}$ protein. A.D.H. prepared the draft of the manuscript. All authors reviewed and edited the manuscript. A.D.H. and T.C. finalized the manuscript.

Competing interests

Authors A.D.H., W.L., Y.-H.J., and T.C. declare the following competing financial interest(s): The authors have the following pending patent related to this manuscript: Chen T, Huber AD, Jung Y-H, Lin W. Non-canonical binding surface that mediates chemical degradation of

nuclear receptors. US Provisional No. 63/783,014. Filed date: April 3, 2025. The remaining authors declare no competing interests.

Additional information

Supplementary information The online version contains supplementary material available at https://doi.org/10.1038/s41467-025-64773-5.

Correspondence and requests for materials should be addressed to Taosheng Chen.

Peer review information *Nature Communications* thanks Gajanan Sathe and the other, anonymous, reviewer(s) for their contribution to the peer review of this work. A peer review file is available.